International Journal of Multiphase Flow 193 (2025) 105371

Contents lists available at ScienceDirect

International Journal of Multiphase Flow

journal homepage: www.elsevier.com/locate/ijmulflow

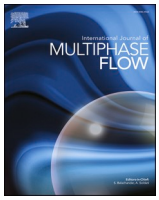

Research Paper

New modeling approaches for liquid holdup and pressure drop in vertical downward gas-liquid two-phase flow

Abderraouf Arabi *, Ronaldo Luis Höhn, Jordi Pallares, Youssef Stiriba

Departament d'Enginyeria Mecànica, Universitat Rovira i Virgili, Av. Països Catalans 26, 43007, Tarragona, Spain

ARTICLE INFO

Keywords:
Gas-liquid two-phase flow
Vertical downward flow
Liquid holdup
Pressure drop
Predictive models

ABSTRACT

The impact of the buoyancy force direction in the different hydrodynamic phenomena occurring, as well as the few numbers of studies carried out, explain the existing complexity in modeling of liquid holdup and pressure drop in vertical downward gas-liquid flow. In this paper, we tackle this challenge through an experimental investigation, a parametric analysis and proposition of new predictive correlations. First a series of experiments were carried out using air-water mixture and 30 mm ID pipe. The experimental results demonstrate the difficulty to model the two parameters using the traditional approaches. Then, using both the present results and data collected from the literature, we propose a new approach that employs liquid-to-gas superficial velocities and input liquid fraction to correlate liquid holdup. Analysis of frictional pressure drop results using the Lockhart-Martinelli approach demonstrates the need to consider a fourth term. This term is originally correlated by means of an analogy with the buoyancy force acting on the Taylor bubbles. The assessment analysis clearly shows that both proposed correlations perform better than existing ones for a large number of data obtained under different flow regimes, pipe diameters and operating conditions. With average absolute relative error values lower than 25 %, both correlations demonstrate their ability to satisfactorily predict data that were not used for their development.

1. Introduction

These recent years, the number of research projects and studies on gas-liquid vertical downward flow has increased thanks to recent interest in reservoir pressure maintenance by the injection of water and gas, microbial enhanced oil recovery (MEOR), carbon capture and storage systems (CCS), or scientific cooling applications that use carbon dioxide (Hammer et al., 2021; Schmid et al., 2022; Bouyahiaoui et al., 2024). This flow orientation is also encountered in nuclear reactors (Lokanathan and Hibiki, 2018; Ayegba et al., 2024b).

Compared to horizontal and vertical upward flows, gas-liquid vertical downward flow remains less studied and less understood. Numerous authors have compared the experimental results of global and local parameters obtained in downward and upward flows (Bhagwat and Ghajar, 2012; Lelouvetel et al., 2014; Chalegri and Jeong, 2019; Bouyahiaoui et al., 2020; Abdulkadir et al., 2021; Hammer et al., 2021; Qiao et al., 2022; Ayegba et al., 2022, 2024a, 2025). The main idea behind these studies is to verify whether current knowledge on vertical upward flow can be extrapolated to vertical downward flow. These studies reported some difference in the hydrodynamic phenomena between the two flow configurations. This difference can be explained by the fact that gravitational and inertia forces act in the opposite direction in vertical downward flow, which influences global and local hydrodynamic phenomena, including the flow regimes. For example, annular flow is present in both ranges of high superficial gas velocity (V_{SG}) and low liquid superficial velocity (V_{SL}) in vertical downward flow; while it is present only in the case of high V_{SG} in vertical upward flow. Also, slug flow occupies a larger zone in vertical upward flow than in vertical downward flow (Qiao et al., 2022). This statement highlights the need to conduct experiments and propose specific models for this pipe orientation.

As well as flow regime, liquid holdup and pressure drop are considered key parameters in the design and control of pipeline systems (Sassi et al., 2020a). These parameters have been less studied compared to vertical upward flow, in terms of available database and developed models. This study targets to contribute to the modeling of the parameters liquid holdup and frictional pressure through a generation of new database as well as the exploration of new approaches for modeling the two parameters. A new dimensionless representation was proposed to model the liquid holdup. Of particularly note is our use of the buoyancy effect term for modeling frictional pressure drop using the

* Corresponding author.
E-mail address: abderraouf.arabi@urv.cat (A. Arabi).

https://doi.org/10.1016/j.ijmultiphaseflow.2025.105371
Received 13 February 2025; Received in revised form 14 July 2025; Accepted 17 July 2025
Available online 18 July 2025

Abbreviation

CCS	Carbone capture and storage
ID	Inner diameter
LBLOCA	Large-break loss of coolant accident
LOCA	Loss of coolant accident
LOHS	Loss of heat sink accident
MEOR	Microbial enhanced oil recovery
PV	Physical parameter
PWR	Pressurized water reactors

Nomenclature

a	Asymmetry coefficient [-]
$AARE$	Average absolute relative error [-]
ARE	Average relative error [-]
B	Buoyancy effect term [-]
b	Empirical coefficent [-]
C	Chisholm parameter [-]
C_0	Distribution coefficient [-]
c	Growth rate [-]
D	Pipe diameter [m]
D_h	Hydraulic diameter [m]
dP/dL	pressure drop gradient [Pa.m^{-1}]
Eo	Eötvös number [-]
F	Frequency [Hz]
f	Friction factor [-]
Fr	Froude number [-]
G	Mass flux [kg.m^{-2}s^{-1}]
g	Gravitational acceleration [m.s^{-2}]
H	Holdup [-]
K	Empirical parameter [-]
L	Length [m]
N	Number of data points [-]
N_μ	Viscosity number [-]
n	Empirical exponent [-]
P	Pressure [Pa]
PM^*	Dimensionless number based on the total pressure drop [-]
R	Calculated parameter
R^2	Coefficient of determination [-]
Re	Reynolds number [-]
$Std(N)$	Standard deviation of the set of N observations [-]
t	Student's statistic appropriate for the number of samples N and the confidence level desired [-]
X	Lockhart-Martinelli parameter [-]
V	Velocity [m.s^{-1}]
Vol	Volume [m^3]
Vol_{ref}	Reference volume [m^3]
Y	Parameter related to the volume of Taylor bubble [-]
Y_1	Parameter related to the liquid holdup [-]
Y_2	Parameter related to the parameter B [-]

Greek letters

δ	Film liquid tickness [m]
ε	Pipe roughness [m]
λ	Input phase fraction [-]
μ	Viscosity [Pa.s]
ρ	Density [kg.m^{-3}]
Φ	Two-phase multiplier [-]

Subscripts

a	Acceleration
cal	Calculated value
exp	Experimental value
f	Darcy-Weisbach friction factor
G	Gas
g	Gravitation
gd	Drift
H	Homogenous
i	Interface
L	Liquid
M	Mixture
O	Only
S	Superficial
tot	Total
TB	Taylor bubble
TP	Two-phase

Conversion

1 cP =	0.001 Pa.s

Lockhart–Martinelli approach.

In the following section, a literature review and discussion on the main experimental available databases of liquid holdup and frictional pressure drop as well as the developed models will be presented.

2. Review of literature on experimental investigation on liquid holdup and frictional pressure drop for vertical downward flow

Table 1 shows the experimental conditions for the most important liquid holdup measurement campaigns conducted for two-phase vertical downward flow. These conditions include fluids, pipe diameter, flow regime, instrumentation and associated uncertainties. One notes that most experiments use an air-water mixture and identify the flow regime. Quick closing valves, on the other hand, are highly popular devices for measuring liquid holdup. Table 1 also shows differences in the terminology used to refer to flow regimes. Usui and Sato (1989), Jiang and Rezkallah (1993), Xue et al. (2016) and Bouyahiaoui et al. (2024) explain that the manner in which liquid holdup is influenced by liquid and gas superficial velocities depends on the nature of the flow regime. Indeed, their studies showed that liquid holdup depends only on liquid superficial velocity in annular and falling film flows, whereas it depends only on gas superficial velocity in bubbly flow. For slug and churn, both liquid and gas superficial velocities affect liquid holdup. This behavior, which is different from that observed in vertical upward flow, may explain the complex influence of the nature of flow regime on liquid holdup in this flow configuration.

As explained by, for example, Vijayan et al. (2000), Woldesemayat and Ghajar (2007) and Márquez-Torres et al. (2020), the large number of liquid holdup correlations developed for horizontal, inclined and vertical upward flows can be divided into four categories: slip ratio, $K\lambda_G$, drift-flux and general correlations. Table 2 compiles the current models developed for vertical downward flow. Note that, except for Yamazaki and Yamaguchi's (1979) model, which was based on $K\lambda_G$ approach, all these models are based on the drift-flux model originally proposed by Zuber and Findley (1965). This approach takes into account all the effects of nonuniform flow and concentration profiles and the effect of the local relative velocity between the phases. The drift-flux model is based mathematically on the expression of gas velocity (V_G) as the product of the distribution coefficient (C_0) and mixture velocity (V_M), plus the drift velocity (V_{gd}) (Eq. (1)).

$$V_G = C_0 V_M - V_{gd} \tag{1}$$

where

Table 1
Summary of existing liquid holdup databases measured in vertical downward gas-liquid two-phase flow.

Authors and year	Fluids used	ID [mm]	Experimental technique used	Liquid holdup uncertainties [%]	Measurement section location [m]	Flow regimes	Data points
Tikhonenko (1973)*	Air-steam (at P = 1.96 MPa and 9.06 MPa)	33	-	-	-	-	57
Usui and Sato (1989)	Air-water	16 and 24	Conductance needle probe	-	1.6 and 2.4	Bubble, slug, churn, annular, and falling film	161
Roustan et al. (1992)	Air-water	50	Quick-closing valves	-	-	-**	30
Jiang and Rezkallah (1993)	Air-water	9.525	Gamma densitometer	-	1.62	Falling film, falling film-annular, annular, froth, churn, slug-churn, slug-froth, slug, bubble-slug, and bubble	95
Kashinsky and Randin (1999)	Air-water	42.3	Electrochemical "blunt-nose'' velocity probe	20	4.44	Bubbly flow	19
Hernandez et al. (2002)	Air-water	50.8	Quick closing valves	-	-	Bubble, slug and annular	91
Sun et al. (2004a)	Air-water	50.8	Four-sensor conductivity probe	10	3.40	Bubbly and bubbly-to-slug transition flows	13
Sun et al. (2004b)	Air-water	50.8	Local multi-sensor conductivity probes	10	3.40	Bubbly and bubbly-to-slug transition flows	5
Ishii et al. (2004)	Air-water	25.4 and 50.8	Conductance type probe	7	3.38 and 3.40	Bubbly	25
Bhagwat and Ghajar (2012)	Air-water	12.7	Quick closing valves	10	-	Falling film, annular, froth, slug and bubbly	66
Vieira et al. (2015)	Air-water and air-water+ Carboxy Methyl Cellulose (CMC)	76	Wire-mesh sensor	5	-	Annular	43
Almabrok et al. (2016)	Air-water	101.6	Wire-mesh sensor	10	4.67	Bubbly, intermittent and annular	67
Xue et al. (2016)	Air-water	25	Quick-closing valves	5.40	Between 1.5 and 4.5	Bubbly, slug, churn and annular	87
Bhagwat and Ghajar (2017)	Air-water	12.7	Quick closing valves	10	-	Falling film, annular, intermittent, slug and transient	29
Wang et al. (2018)	Air-water	203.2	Impedance void meter	10	14.83	Cap bubbly, churn-turbulent and annular***	56
Li et al. (2018)	Air-water	203.2	Impedance void meter	10	14.83	Cap bubbly, churn-turbulent and annular	6
Chalgeri and Jeong (2019)	Air-water	66.5 × 2.35 (D_h= 4.55)	Electrical impedance	-	-	Bubbly, large bubbly, cap bubbly, slug, churn-turbulent, annular, falling film and undefined	290
Hazuku et al. (2020)	Nitrogen-water	1.03, 3 and 5	High-speed camera	15	0.15, 0.45 and 0.55	Bubbly	13
Bouyahiaoui et al. (2020)	Air-water	34	Conductance probe	-	5.9	Churn	40
Shi et al. (2021)	Air-water	20	Quick-closing valves	-	-	****	167
Olarinoye (2021)	Air-water	127	Conductance ring probes	-	-	Annular	86
Hammer et al. (2021)	CO_2	44	Broad-beam gamma densitometer	0.02	1.11	Annular bubble, bubble, cap bubble, churn, and droplet	34
Ualiyeva et al. (2022)	Air-oil	50.8	Quick-closing valves	-	-	Falling film, liquid slip, and wavy annular	42
Osuagwu (2024)	Air-water	50.8	Quick-closing valves	-	-	Slug, churn and annular	75

* Taken from Blinkov et al. (2022).
** Experiments carried out with bubble and bubble-to-slug transition flow. The nature of the flow regime of the data was not reported.
*** Taking into account that the experimental setup is the same as that used by Li et al. (2018).
**** Experiments carried out with falling film, bubble, slug, transition and annular. The nature of the flow regime of the data was not reported.

$$V_G = \frac{V_{SG}}{1 - H_L}, \tag{2}$$

$$V_M = V_{SG} + V_{SL} \tag{3}$$

Note the negative value of the drift velocity is a consequence of the direction of the buoyancy force in the vertical downward flow. If this approach is based on physics, the drift-flux parameters (C_0 and V_{gd}) are obtained by employing empirical approaches, which depends to the experimental results obtained ad hoc and the parametric study conducted. Clark and Flemmer (1984) and Bouyahiaoui et al. (2020), for instance, proposed constant values of the two drift-flux parameters, whereas the other models considered the physical properties of the fluids. In the models of Hirao et al. (1986), Goda (2001) and Goda et al. (2003), the influence of the gas and liquid superficial velocities on the distribution coefficient is quantified through the mixture velocity, whereas in the recent models of Dong and Hibiki (2021), Shi et al. (2021) and Hwang et al. (2023) the superficial velocities of the two phases are considered separately.

Wang et al. (2018) modified the model of Goda et al. (2003) for $H_L <$ 0.7. This modification was done after that Wang et al. (2018) observed a shift in the predictions level of the model of Goda et al. (2003) with their data obtained with 203.2 mm ID. Shi et al. (2021) correlated the drift velocity for each flow regime separately using their generated database

Table 2
Summary of existing liquid holdup predictive models for gas-liquid vertical downward flow.

Authors and year	Correlation
Yamakazi and Yamaguchi (1979)	$\frac{1-H_L}{H_L(1-K(1-H_L))}=\frac{\lambda_G}{1-\lambda_G}$ $\lambda_G=\frac{V_{GS}}{V_{GS}+V_{LS}}$ $K=\begin{cases}2-0.4/\lambda_G for\ \lambda_G\le 0.2\\ -0.25+1.25\lambda_G\ for\ \lambda_G\ge 0.2\end{cases}$
Clark and Flemmer (1984)	$C_0=1.165$ $V_{gd}=0.24$
Hirao et al. (1986)	$C_0=\begin{cases}0.9+0.1\sqrt{\frac{\rho_G}{\rho_L}}\ for\ V_M\le 2.5\ m/s\\ 0.9+0.1\sqrt{\frac{\rho_G}{\rho_L}}-0.3\left(1-\sqrt{\frac{\rho_G}{\rho_L}}\right)(2.5-V_M)\ for\ 3.5\le V_M\le 3.5\ m/s\\ 1.2-0.2\sqrt{\frac{\rho_G}{\rho_L}}\ for\ V_M>3.5\ m/s\end{cases}$ $V_{gd}=\sqrt{2}\left(\frac{g\sigma(\rho_L-\rho_G)}{\rho_L^2}\right)^{0.25}$
Kataoka and Ishii (1987)	$C_0=1.2-0.2\sqrt{\frac{\rho_G}{\rho_L}}$ $V_{gd}=\begin{cases}0.0019D^{*0.809}\left(\frac{\rho_G}{\rho_L}\right)^{-0.157}N_{\mu L}^{-0.562}\left(\frac{g\sigma(\rho_L-\rho_G)}{\rho_L^2}\right)^{0.25}\ for\ N_{\mu L}\le 2.2\times 10^{-3}and\ D^*\le 30\\ 0.030\left(\frac{\rho_G}{\rho_L}\right)^{-0.157}N_{\mu L}^{-0.562}\left(\frac{g\sigma(\rho_L-\rho_G)}{\rho_L^2}\right)^{0.25}\ for\ N_{\mu L}\le 2.2\times 10^{-3}and\ D^*>30\\ 0.92\left(\frac{\rho_G}{\rho_L}\right)^{-0.157}\left(\frac{g\sigma(\rho_L-\rho_G)}{\rho_L^2}\right)^{0.25}\ for\ N_{\mu L}\ge 2.2\times 10^{-3}\end{cases}$ $N_{\mu L}=\frac{\mu_L}{\left(\rho_L\sigma\sqrt{\frac{\sigma}{g(\rho_L-\rho_G)}}\right)^{0.5}}$ $D^*=\frac{D}{\sqrt{\frac{\sigma}{g(\rho_L-\rho_G)}}}$
Usui and Sato (1989)	$C_0=1.2-\frac{1}{2.95+350Eo^{-1.3}}$ $V_{gd}=0.345\left(1-\exp\left(\frac{3.37-Eo}{10}\right)\right)$ $Eo=\frac{g(\rho_L-\rho_G)D^2}{\sigma}$
Goda (2001)	$C_0=\begin{cases}0.9+0.1\sqrt{\frac{\rho_G}{\rho_L}}\ for\ \sqrt{2}V_M\left(\frac{g\sigma(\rho_L-\rho_G)}{\rho_L^2}\right)^{0.25}\le 13\\ 0.9+0.1\sqrt{\frac{\rho_G}{\rho_L}}-\left(1-\sqrt{\frac{\rho_G}{\rho_L}}\right)\left(0.45-0.0495\sqrt{2}V_M\left(\frac{g\sigma(\rho_L-\rho_G)}{\rho_L^2}\right)^{0.25}\right)\ for\ 13\ge\sqrt{2}\left(\frac{g\sigma(\rho_L-\rho_G)}{\rho_L^2}\right)^{0.25}\ge 22\\ 1.26-0.26\sqrt{\frac{\rho_G}{\rho_L}}-0.26\left(1-\sqrt{\frac{\rho_G}{\rho_L}}\right)\left(1-exp\left(0.014V_M\left(\frac{g\sigma(\rho_L-\rho_G)}{\rho_L^2}\right)^{0.25}\right)\right)\ for\ V_M>22\end{cases}$ $V_{gd}=\sqrt{2}\left(\frac{g\sigma(\rho_L-\rho_G)}{\rho_L^2}\right)^{0.25}$
Goda et al. (2003)	$C_0=\begin{cases}\left(0.772+0.0214\frac{V_M}{\sqrt{2}\left(\frac{g\sigma(\rho_L-\rho_G)}{\rho_L^2}\right)^{0.25}}\right)+\left(0.228-0.0214\frac{V_M}{\sqrt{2}\left(\frac{g\sigma(\rho_L-\rho_G)}{\rho_L^2}\right)^{0.25}}\right)\sqrt{\frac{\rho_G}{\rho_L}}\ for\ \frac{V_M}{\sqrt{2}\left(\frac{g\sigma(\rho_L-\rho_G)}{\rho_L^2}\right)^{0.25}}\le 20\\ \left(1.0+0.2exp\left(0.0848\left(20-\frac{V_M}{\sqrt{2}\left(\frac{g\sigma(\rho_L-\rho_G)}{\rho_L^2}\right)^{0.25}}\right)\right)\right)-0.2exp\left(0.0848\left(20-\frac{V_M}{\sqrt{2}\left(\frac{g\sigma(\rho_L-\rho_G)}{\rho_L^2}\right)^{0.25}}\right)\right)\sqrt{\frac{\rho_G}{\rho_L}}\ for\ \frac{V_M}{\sqrt{2}\left(\frac{g\sigma(\rho_L-\rho_G)}{\rho_L^2}\right)^{0.25}}>20\end{cases}$ $V_{gd}=\sqrt{2}\left(\frac{g\sigma(\rho_L-\rho_G)}{\rho_L^2}\right)^{0.25}$
Wang et al. (2018)	$C_0=\begin{cases}\left(0.772+0.0214\frac{V_M}{\sqrt{2}\left(\frac{g\sigma(\rho_L-\rho_G)}{\rho_L^2}\right)^{0.25}}\right)+\left(0.228-0.0214\frac{V_M}{\sqrt{2}\left(\frac{g\sigma(\rho_L-\rho_G)}{\rho_L^2}\right)^{0.25}}\right)\sqrt{\frac{\rho_G}{\rho_L}}\ for\ \frac{V_M}{\sqrt{2}\left(\frac{g\sigma(\rho_L-\rho_G)}{\rho_L^2}\right)^{0.25}}\le 20\\ \left(1.0+0.2exp\left(0.0848\left(20-\frac{V_M}{\sqrt{2}\left(\frac{g\sigma(\rho_L-\rho_G)}{\rho_L^2}\right)^{0.25}}\right)\right)\right)-0.2exp\left(0.0848\left(20-\frac{V_M}{\sqrt{2}\left(\frac{g\sigma(\rho_L-\rho_G)}{\rho_L^2}\right)^{0.25}}\right)\right)\sqrt{\frac{\rho_G}{\rho_L}}\ for\ \frac{V_M}{\sqrt{2}\left(\frac{g\sigma(\rho_L-\rho_G)}{\rho_L^2}\right)^{0.25}}>20\end{cases}$ $V_{gd}=\begin{cases}3\left(\frac{g\sigma(\rho_L-\rho_G)}{\rho_L^2}\right)^{0.25}\ for\ H_L<0.7\\ \sqrt{2}\left(\frac{g\sigma(\rho_L-\rho_G)}{\rho_L^2}\right)^{0.25}\ for\ H_L>0.7\end{cases}$

(continued on next page)

Table 2 (*continued*)

Authors and year	Correlation
Bouyahiaoui et al. (2020)	$C_0 = 1.288$ $V_{gd} = 0.7358$
Dong and Hibiki (2021)	$C_0 = \{ \begin{matrix} 0.9exp\left(0.286\left(\frac{\lambda_G}{0.9}\right)^{1.5}\right) - \left[0.9exp\left(0.286\left(\frac{\lambda_G}{0.9}\right)^{1.5}\right) - 1\right]\sqrt{\frac{\rho_G}{\rho_L}} \text{ for } \lambda_G \le 0.9 \\ (3-2\lambda_G) - (2-2\lambda_G)\sqrt{\frac{\rho_G}{\rho_L}} \text{ for } \lambda_G > 0.9 \end{matrix}$ $V_{gd} = \sqrt{2}\left(\frac{g\sigma(\rho_L-\rho_G)}{\rho_L^2}\right)^{0.25}$
Shi et al. (2021)	$C_0 = 1 + 0.16\left(1 - \frac{\rho_G V_G}{\rho_G V_G + \rho_L V_L}\right)$ $V_{gd} = \{ \begin{matrix} 0.01\left(\frac{g\sigma(\rho_L-\rho_G)}{\rho_L^2}\right)^{0.25} \text{ for falling film flow} \\ -0.85\left(\frac{g\sigma(\rho_L-\rho_G)}{\rho_L^2}\right)^{0.25} \text{ for bubble flow} \\ 0.47\left(\frac{g\sigma(\rho_L-\rho_G)}{\rho_L^2}\right)^{0.25} \text{ for slug flow} \\ -0.73\left(\frac{g\sigma(\rho_L-\rho_G)}{\rho_L^2}\right)^{0.25} \text{ for transition flow} \\ -0.63\left(\frac{g\sigma(\rho_L-\rho_G)}{\rho_L^2}\right)^{0.25} \text{ for annular flow} \end{matrix}$
Hwang et al. (2023)	$C_0 = exp(0.3758\lambda_G^{0.02}) - \left[exp(0.3758\lambda_G^{0.02}) - 1\right]\sqrt{\frac{\rho_G}{\rho_L}}$ $V_{gd} = \sqrt{2}\left(\frac{g\sigma(\rho_L-\rho_G)}{\rho_L^2}\right)^{0.25}$

obtained with 20 mm ID. This model can therefore be used only when the nature of the flow regime is known. Note that Shi et al. reported positive values of drift velocity for some regimes but did not present any explanations for these findings. In the same year, Dong and Hibiki (2021) collected a database composed of 1252 liquid holdup measurements obtained from 13 sources. By employing the approach of Hibiki and Ishii (2003), Dong and Hibiki (2021) proposed a new drift-flux model that has a larger applicability range than existing ones.

As a summary, the difference in the manner in which the liquid holdup was correlated can explain the difficulty in correlating liquid holdup in vertical downward flow. Further efforts are therefore needed to advance our knowledge on the correlation of liquid holdup in this flow configuration.

On the other hand, the total pressure drop $\left(\left(\frac{dP}{dL}\right)_{tot,\ TP}\right)$ is the sum of three components: gravitational pressure drop $\left(\left(\frac{dP}{dL}\right)_{g,TP}\right)$, frictional pressure drop $\left(\left(\frac{dP}{dL}\right)_{f,\ TP}\right)$, and acceleration pressure drop $\left(\left(\frac{dP}{dL}\right)_{a,TP}\right)$, as given in Eq. (4) (Lu et al., 2018).

$$\left(\frac{dP}{dL}\right)_{tot,\ TP} = \left(\frac{dP}{dL}\right)_{g,TP} - \left(\frac{dP}{dL}\right)_{f,\ TP} + \left(\frac{dP}{dL}\right)_{a,TP} \tag{4}$$

In the above equation note the negative sign of frictional pressure drop in vertical downward flow. This can be explained by the fact that the frictional pressure drop has a different sign from the total pressure gradient in this flow orientation. The contribution of the third term in Eq. (4) is negligible in adiabatic two-phase flow and is generally ignored (Bouyahiaoui et al., 2024; Höhn et al., 2025b). The gravitational pressure drop term in vertical configuration is calculated as follows (Bouyahiaoui et al., 2024; Höhn et al., 2025b):

$$\left(\frac{dP}{dL}\right)_{g,TP} = \rho_{TP} g = (H_L\rho_L + (1-H_L)\rho_G)g \tag{5}$$

where ρ_{TP} and g are the gas-liquid mixture density and gravitational acceleration, respectively.

The current existing database for vertical frictional pressure drop in vertical downward flow is summarized in Table 3. Most publicly available databases for pressure drop are obtained using an air-water mixture and taking into account the nature of flow regimes.

Separated flow model is still the most popular approach for modeling the vertical downward frictional pressure drop. With this approach, the frictional pressure drop is expressed as a function of liquid pressure drop $\left(\left(\frac{dP}{dL}\right)_L\right)$ or liquid-only pressure drop $\left(\left(\frac{dP}{dL}\right)_{LO}\right)$. These single-phase pressure drops are expressed as:

$$\left(\frac{dP}{dL}\right)_L = \frac{f_L G_L^2}{2D\rho_L} \tag{6}$$

$$\left(\frac{dP}{dL}\right)_{LO} = \frac{f_{LO} G_{TP}^2}{2D\rho_L} \tag{7}$$

In Eqs. (6) and (7), G_L and G_{TP} stand for liquid and total mass fluxes, while f_L and f_{LO} are the Darcy-Weisbach friction factors for liquid and liquid-only, respectively. The mass fluxes of liquid and gas phase are calculated as:

$$G_L = \rho_L V_{SL} \tag{8}$$

$$G_G = \rho_G V_{SG} \tag{9}$$

The total mass flux is the sum of the liquid and gas mass fluxes (Eq. (10)).

$$G_{TP} = G_L + G_G = \rho_L V_{SL} + \rho_G V_{SG} \tag{10}$$

f_L (or f_{LO}) is calculated iteratively or explicitly by taking into account Re_L (or Re_{LO}) and pipe roughness (ε) from the various friction factor correlations available. The Reynolds numbers Re_L and Re_{LO} are given by

$$Re_L = \frac{G_L D}{\mu_L} \tag{11}$$

$$Re_{LO} = \frac{G_{TP} D}{\mu_L} \tag{12}$$

The frictional pressure drop is calculated by taking into account the liquid and liquid-only pressure drop in Eqs. (13) and (14), respectively.

Table 3
Summary of existing frictional pressure drop databases measured in vertical downward gas-liquid two-phase flow.

Authors and year	Fluids used	ID [mm]	**Pressure drop uncertainty**	**Pressure taps location [m]**	Flow regimes	Data points
Roustan et al. (1992)	Air-water	50	-	-	-*	30
Lau and Rezkallah (1995)	Air-water	9.53	8 %	0.667 and 1.24	Falling film, annular, froth, slug-annular, slug, bubble-slug, bubble, bubble-froth and slug-annular-froth	103
Sun et al. (2004a)	Air-water	50.8	1 %	-	Bubbly, and bubbly-to-slug transition	13
Bhagwat et al. (2012)	Air-water	12.5	6.5 %	-	Bubbly, slug, froth, annular and falling film	152
Xue et al. (2013)	Air-water	65	-	-	Bubbly, slug, and churn	90
Almabrok (2013)	Air-water	101.6	0.08 %	1.02 and 5.08	Bubbly, intermittent and annular	135
Lu et al. (2018)	Air-water	50.8	0.1 %	2.06 and 3.43	Bubbly, transitional and slug	18
Ualiyeva et al. (2022)	Air-oil	50.8	-	-	Falling film, liquid slip, and wavy annular	42
Bouyahiaoui et al. (2024)	Air-water	34	0.1 %	3.50 and 4.54	Falling film, annular, bubbly, cap bubble, slug, and churn	131

* Experiments carried out with bubble and bubble-to-slug transition flow. The nature of the flow regime of the data was not reported.

Table 4
Summary of existing frictional pressure drop predictive models for gas-liquid vertical downward flow.

Authors and year	Correlation
Yamakazi and Yamaguchi (1979)	$\Phi_L = H_L^{-0.9}$
Friedel (1979)	$\Phi_{LO}^2 = (1-\dot{x})^2 + \dot{x}^2 \frac{\rho_L}{\rho_G}\frac{f_{GO}}{f_{LO}} + 48.6 \frac{\dot{x}^{0.8}(1-\dot{x})^{0.29}\left(\frac{\rho_L}{\rho_G}\right)^{0.9}\left(\frac{\mu_G}{\mu_L}\right)^{0.73}\left(1-\frac{\mu_G}{\mu_L}\right)^{7.4} Fr_F^{0.03}}{We_F^{0.12}}$ $\dot{x} = \frac{G_G}{G_{TP}}$ $Fr_F = \frac{G_{TP}^2}{\rho_{TPH}^2 gD}$ $We_F = \frac{G_{TP}^2 D}{\rho_{TPH}\sigma}$ $\rho_{TPH} = \left[\frac{\dot{x}}{\rho_G} + \frac{1-\dot{x}}{\rho_L}\right]^{-1}$ $f_{LO} = \begin{cases} 64/Re_{LO} \text{ for laminar flow} \\ \left[0.86859 ln\left(\frac{Re_{LO}}{1.964 Re_{LO} - 3.8215}\right)\right]^{-2} \text{ for turbulent flow} \end{cases}$ $f_{go} = \begin{cases} 64/Re_{GO} \text{ for laminar flow} \\ \left[0.86859 ln\left(\frac{Re_{GO}}{1.964 Re_{GO} - 3.8215}\right)\right]^{-2} \text{ for turbulent flow} \end{cases}$
Lau and Rezkallah (1995)	$\phi_L^2 = \begin{cases} H_L^{-1.14} \text{ for } H_L > 0.1 \\ 1.23 \times 10^{-5} Re_{SL}^{1.04}\left(\frac{V_{SG}}{V_{SL}}\right)^{1.26} \text{ for annular flow} \end{cases}$
Qiao et al. (2017)	$\phi_L^2 = 1 + \frac{25}{X} + \frac{1}{X^2}$ $\phi_L^2 = 1 + \frac{100}{X} + \frac{1}{X^2}$
Yao et al. (2018)	$\phi_L^2 = 1 + \frac{C}{X} + \frac{1}{X^2} + B$ $C = \begin{cases} 5 \text{ for viscous liquid} - \text{viscous gas flow} \\ 10 \text{ for turbulent liquid} - \text{viscous gas flow} \\ 12 \text{ for viscous liquid} - \text{turbulent gas flow} \\ 20 \text{ for turbulent liquid} - \text{turbulent gas flow} \end{cases}$ $B = 36.371\left[\left(\frac{gD}{V_{LS}^2}\right)\left(1-\frac{\rho_G}{\rho_L}\right)\right]^{1.278} 0.995\left[X - \left(\frac{\rho_L}{\rho_G}\right)^{-0.01}\left(\frac{\mu_L}{\mu_G}\right)^{0.77}\left(\frac{\sqrt{gD}}{V_{SL}}\right)^{0.41}\right]^2$
Lu et al. (2018)	$\Phi_L^2 = 1 + \frac{50}{X} + \frac{1}{X^2}$ $H_L^{-0.875}$
Hwang et al. (2024)	$\Phi_L^2 = 1 + \frac{652}{X} + \frac{1}{X^2}$

$$\left(\frac{dP}{dL}\right)_{f,TP} = \phi_L^2 \left(\frac{dP}{dL}\right)_L \tag{13}$$

$$\left(\frac{dP}{dL}\right)_{f,TP} = \phi_{LO}^2 \left(\frac{dP}{dL}\right)_{LO} \tag{14}$$

where ϕ_L^2 and ϕ_{LO}^2 are known as two-phase multipliers.

Several empirical models have been developed to predict the two-phase multipliers. These are summarized in Table 4. Yamazaki and Yamaguchi (1979) correlated the two-phase flow multiplier with the liquid holdup using a power law function. The liquid holdup is thus calculated using their model shown in Table 2. Using the same methodology, Lau and Rezkallah (1995) and Lu et al. (2018) reported other values of the exponent. Lau and Rezkallah (1995) also noted that this correlation is not valid when $H_L < 0.1$, which corresponds to the annular flow. They therefore proposed a specific correlation for this flow regime. Friedel (1979) developed his model by using a database made up of 1311 experimental points obtained with air-water, air-oil and steam-air mixtures and important range of hydraulic diameters (5–51 mm). His model recourses to several dimensionless numbers.

All remaining models displayed in Table 4 are based on Chisholm's (1967) methodology, which is built on the fact that the frictional pressure drop is the sum of the pressure drop generated by the liquid phase, the gas phase $\left(\left(\frac{dP}{dL}\right)_G\right)$, and the interfacial interaction between both phases $\left(\left(\frac{dP}{dL}\right)_i\right)$ (Eq. (15)) (Muzychka and Awad, 2010).

$$\left(\frac{dP}{dL}\right)_f = \left(\frac{dP}{dL}\right)_L + \left(\frac{dP}{dL}\right)_G + \left(\frac{dP}{dL}\right)_i \tag{15}$$

If we divide Eq. (15) by the liquid pressure drop, we obtain the equation of the two-phase flow multiplier (Eq. (16)).

$$\Phi_L^2 = 1 + \frac{C}{X} + \frac{1}{X^2} \tag{16}$$

where C and X refer to the Chisholm parameter and Lockhart-Martinelli parameter, respectively. According to Chisholm's (1967) pioneering correlation, the Chisholm parameter is given as:

$$C = \begin{cases} 5 \text{ for viscous liquid} - \text{viscous gas flow} \\ 10 \text{ for turbulent liquid} - \text{viscous gas flow} \\ 12 \text{ for viscous liquid} - \text{turbulent gas flow} \\ 20 \text{ for turbulent liquid} - \text{turbulent gas flow} \end{cases} \tag{17}$$

The Lockhart-Martinelli parameter is calculated from Eq. (18).

$$X = \sqrt{\frac{\left(\frac{dP}{dL}\right)_L}{\left(\frac{dP}{dL}\right)_G}} \tag{18}$$

Qiao et al. (2017), Lu et al. (2018) and Hwang et al. (2024) proposed different values of C. Qiao et al. (2017), for example, reported that the Chisholm parameter depends strongly on the inlet injector. A specific value of C was therefore proposed for each inlet geometry configuration. Note that their experiments were carried out for bubbly flow. Lu et al. (2018) obtained $C = 50$ using their database collected under bubbly, bubbly-to-slug and slug flows conditions. Note that both studies of Qiao et al. (2017) and Lu et al. (2018) used the same pipe diameter of 50.8 mm. On the other hand, Hwang et al. (2024) employed a large pipe diameter of 600 mm. The recourse to a unique value of Chisholm parameter has been questioned by Muzychka and Awad (2010) and recently Höhn et al. (2025b) for horizontal and vertical upward flow orientations, respectively.

Note that the Lu et al. (2018) also found that the value of C in downward two-phase flow is greater than that in vertical upward flow, which means that the vertical downward flow generates higher frictional losses. According to Yao et al. (2018), the higher value of the frictional pressure drop in vertical downward flow is explained by the buoyancy force acting on gas bubbles. This force is opposite to the inertia and induces additional frictional losses. Yao et al. (2018) added a fourth term to Eq. (16) to include this physical effect. These authors correlated this additional term by using data they obtained with four pipe diameters (15, 25, 40 and 65 mm). Note that they considered the values proposed by Chisholm (1967) for the Chisholm parameter. According to the recent study by Blinkov et al. (2022), the modeling approach of Yao et al. (2018) should be considered a way to improve the modeling of frictional pressure drop in vertical downward two-phase flow. Note that all the correlations reported in Table 4 have not been validated with independent data. Some doubts may therefore arise over their applicability and validity in ranges of conditions that fall outside those for the data used for their development.

Bouyahiaoui et al. (2024) recently compared data generated with an air-water mixture and a 34 mm ID to the predictions provided by the models of Yamakazi and Yamaguchi (1979), Friedel (1979), Yao et al. (2018), and Lu et al. (2018). These authors found that the prediction level of each model depends strongly on the nature of the flow regime. Note that they reported large relative errors between the measured and the calculated frictional pressure drops. This highlights the limitations of the current correlations and the need for developing new models.

3. Experimental setup

This study was conducted using the LESLIE (Low prESsure muLtI-phasE test loop) experimental setup developed by the ECOMMFIT research group of Universitat Rovira i Virgili (Tarragona, Spain). This setup, which is illustrated in Fig. 1a, was developed for studying gas-liquid two-phase and gas-liquid-solid three-phase flows for different pipe orientations, has been used in numerous studies (Sassi et al., 2020a, 2020b, 2022; Höhn et al., 2025a). It comprises four parts (horizontal, vertical upward, horizontal and vertical downward sections) that are made from clear acrylic, have an inner diameter of 30 mm, and are connected with three bends whose radius of curvature is 219.9 mm.

Tap water and compressed air were used as the test fluids. The liquid and gas phases flow through closed and open circuits, respectively. The water is pumped from a tank using a 5.5 kW Weir model AB80 centrifugal pump with an open impeller. The water flow rate was controlled and measured with a WEG CFW 500 variable frequency drive (VFD) and an Isoil MS2500 electromagnetic flow meter (with an accuracy of ±0.8 %), respectively. An Omega controller with an accuracy of ±0.8 % was used to control and measure the air mass flowmeter. The gas-water mixture flows into the four parts and reaches the tank, which also works as a separator at atmospheric pressure. All experiments were conducted at atmospheric pressure and ambient temperature (22±3°C).

This study examines the vertical downward flow section, which is 2.99 m in length. The test section is equipped with three quick-closing valves to trap the gas-liquid mixture in two sections. As was discussed in Section 2, this is still a popular technique for measuring liquid holdup. For each condition, several measurements of liquid holdup were carried out and their calculated average was considered as the liquid holdup value. The vertical downward section is also equipped with four absolute pressure transducers with an accuracy of 0.3 %. The signals from the four transducers are sampled simultaneously using a Keysight U2542A USB data acquisition system. For each experimental condition, a time series with a length of 60 s is collected at a frequency of 1000 Hz. The detailed positions of the pressure transducers and quick-closing valves, reported from the end of the bend, are shown in Fig. 1b. Flow visualization was performed using a high-speed Photron FASTCAM mini UX100 type 800 K camera placed at ≈ 87D from the start of the vertical downward pipe. As we discuss in Section 4.4.1, the two-phase flow is fully developed at this location.

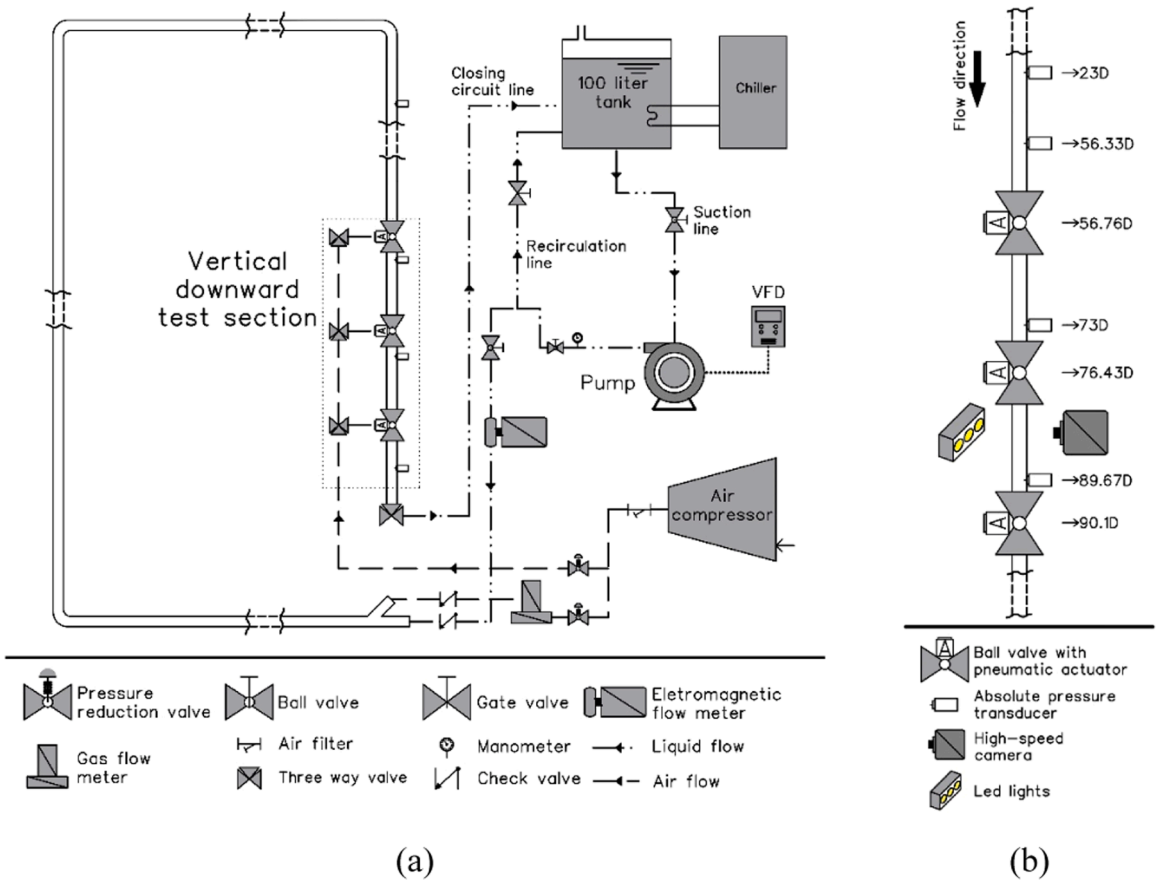

Fig. 1. Schematic diagram of (a) the overall LESLIE setup, and (b) the vertical downward section used in this study.

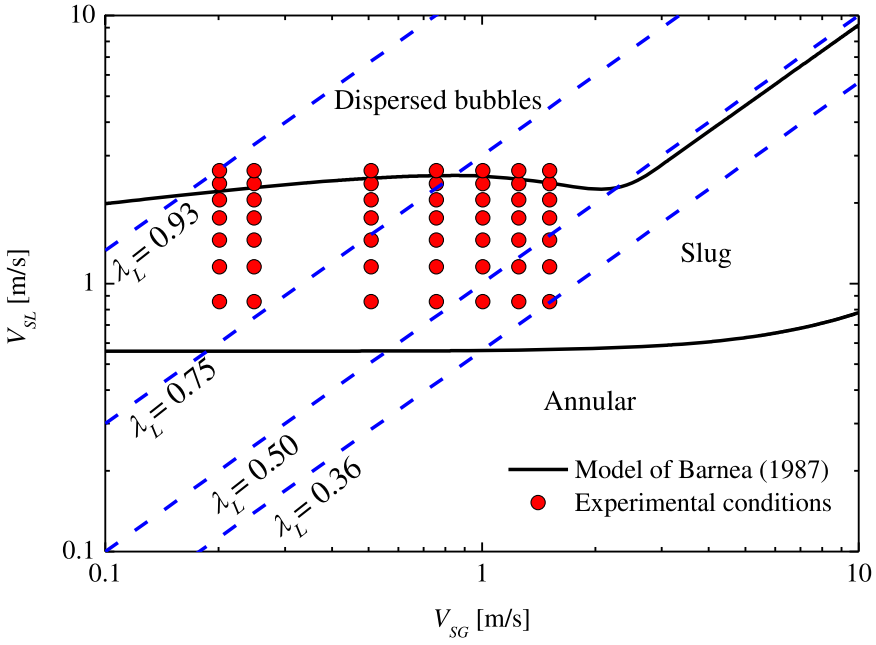

Fig. 2. Plot of the experimental conditions in Barnea's (1987) general flow map obtained using FLOPATN. The iso-input liquid holdup lines are also depicted.

For the calculated superficial velocities and pressure drops, the uncertainty of each calculated parameter R (δR) was calculated by considering the uncertainties of all the individual measured parameters (X_1, X_2, X_3, …, X_n) used in the calculation of the computed parameter. This was done by using a root-sum square combination of the effects of each of the individual input measured parameters as shown in Eq. (19) (Moffat, 1988).

$$\delta R = \sqrt{\sum_{i=1}^{N} \left(\frac{\delta R}{\delta X_i} \delta X_i \right)^2} \tag{19}$$

On the other hand, the uncertainty associated with the liquid holdup measurements for each condition were calculated using the following formula (Moffat, 1988):

$$\delta H_L = \frac{t\ Std_{(N)}}{\sqrt{N}} \tag{20}$$

where $Std_{(N)}$ is the standard deviation of the set of N observations used to calculate the mean value of liquid holdup, and t is the Student's statistic appropriate for the number of samples N and the confidence level desired. In our study, the confidence level of 90 % was chosen. Further details on Student's t-test can be found in De Wineter (2013), Montgomery and Runger (2010), Devore and Carlton (2016) and Li and Nadarajah (2020). The uncertainty of liquid holdup was found between 0.53 % and 15.44 % with a mean value of 5.00 %.

In total, 49 experimental conditions, corresponding to 0.86 m/$s \leq V_{SL} \leq$ 2.63 m/s and 0.20 m/$s \leq V_{SG} \leq$ 1.51 m/s, were analyzed. Fig. 2 plots the experimental conditions for this study on Barnea's (1987) flow map generated using FLOPATN (Pereyra and Torres, 2005). Barnea's flow map is a unified mechanistic flow map for all pipe inclinations. Fig. 2 shows that most experimental points were located in the area of slug flow. In the present experiments the dispersed bubbly flow was not observed. This means that the model underestimated the critical V_{SL} for the slug-to-dispersed bubble flow transition for this case. The plots of the iso-input liquid fraction (calculated using Eq. 21) show that this experiment covers an important range of high-input liquid fraction (0.36 $\leq \lambda_L \leq$ 0.93) and that, for most points, $\lambda_L \geq$ 0.50. Note that most existing data for the range of high-input liquid fractions are obtained in the bubbly flow regime.

$$\lambda_L = \frac{V_{SL}}{V_M} \tag{21}$$

4. Results and discussion

The images obtained with the high-speed camera were used to identify the flow regimes. The results for liquid holdup and total and frictional pressure drop are discussed after. Note that single-phase measurements are used to validate those for two-phase flow pressure drop. The results from this step are presented before those for two-phase flow total pressure drop.

4.1. Flow regimes visualization and identification

Due to the importance of flow regimes for liquid holdup and pressure drop (discussed in Section 2), we paid special attention to flow regime visualization and identification, by observing and analyzing images captured with the high-speed camera.

In the range of flow conditions covered by this study, three flow regimes were observed (Fig. 3):

a. *Cap bubble flow*. This flow can be viewed as a continuous liquid phase transporting small dispersed bubbles, bubble clusters, and cap bubbles. The presence of cap bubbles is mainly due to the greater number of dispersed small gas bubbles and their coalescence. This flow regime is a transition between bubbly and slug flows.
b. *Slug flow*. Like cap bubble flow, this flow is a succession of elongated bubble and liquid slugs. However, the elongated bubbles in slug flow are longer than the cap bubbles. "Taylor bubble" is the term used to refer to them. In vertical downward flow, Taylor bubbles have an asymmetrical nose that points in the opposite direction to the flow.
c. *Churn flow*. This flow sees the progressive disappearance of liquid slugs and Taylor bubbles and the presence of a turbulent liquid bridge that transports a large number of gas bubbles, similar to foam flows. These phenomena are caused by an increase in gas turbulence level that causes the transition to annular flow. Indeed, churn flow is a transitionary regime between slug and annular flows. Note that this flow regime is also known in the literature as churn-turbulent, foam or froth flows.

The experimental conditions of these flow regimes are plotted in Fig. 4a alongside the flow transition lines obtained by Qiao et al. (2017), whose flow regime map was constructed from experiments conducted with an air-water mixture and a 50.8 mm ID pipe and, as in our study, the vertical downward flow was fed from a horizontal pipe. Fig. 4a shows that the cap bubble flow was present in the range of high and low liquid and gas superficial velocities, respectively, and occupies the slug flow zone near the transition to bubbly flow. This may be because, as previously discussed, this flow regime represents a transition between these two flow regimes. Churn flow, on the other hand, occupies the zones for high gas flow rates. A satisfactory prediction is shown between the observed flow regimes and the predictions of the flow pattern map.

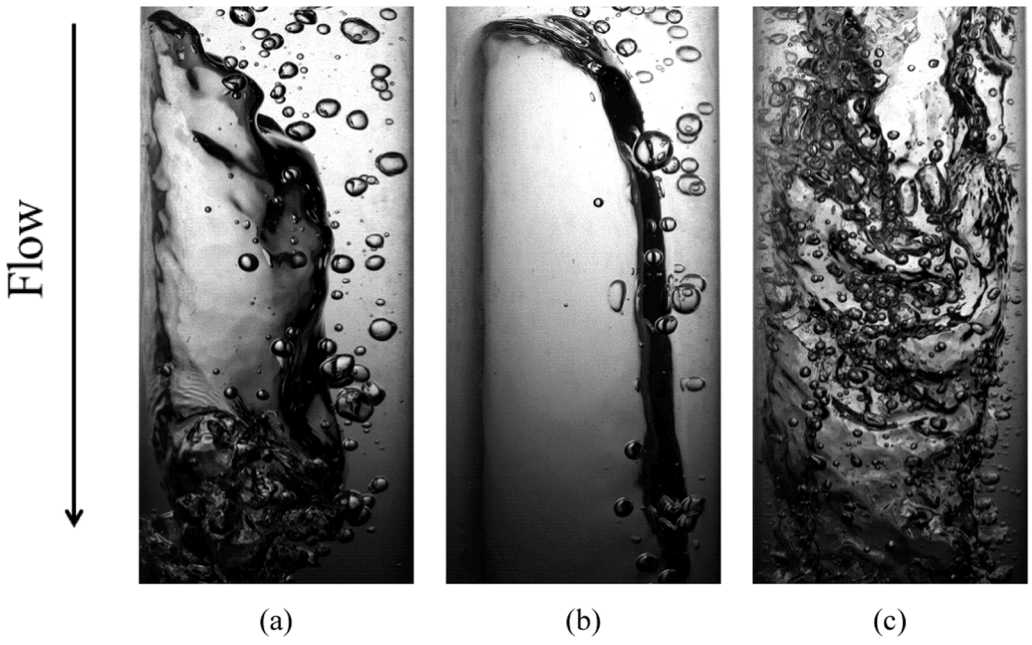

Fig. 3. Images of (a) cap bubble flow, (b) slug flow, and (c) churn flow observed in the present experiments.

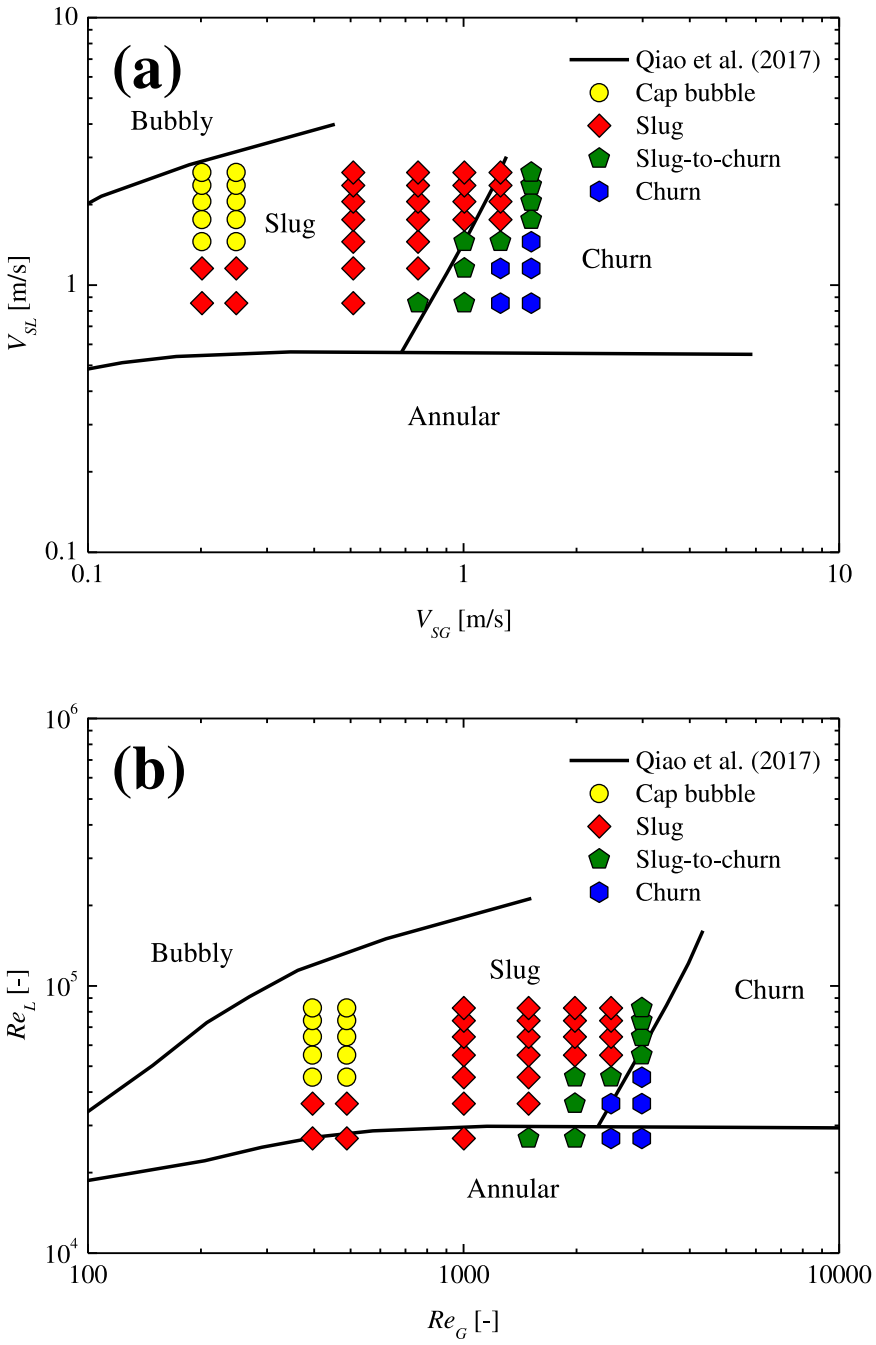

Fig. 4. Plot of the experimental conditions for each flow regime observed in the flow pattern map of Qiao et al. (2017) using (a) V_{SL} vs V_{SG}; and (b) Re_L vs Re_G coordinates systems.

The deviation observed between slug and churn flows may be explained by the difference in pipe diameter between our experimental setup and that used by Qiao et al. (2017). To confirm this hypothesis, the flow conditions and the flow transition lines of Qiao et al. (2017) are plotted in Fig. 4b using the Re_L vs Re_G coordinate system. It appears that this plot allows to better capture the influence of gas flow rate on the slug-to-churn flow transition. However, this coordinate system fails to predict the annular-to-intermittent flow transition.

4.2. Liquid holdup

This section analyzes the liquid holdup measured for the various flow regimes. Our analysis includes the effect of liquid and gas superficial velocities and the homogenous and drift-flux models. An original empirical method is proposed to predict this parameter. The predictions made by the current model and this new model will then be compared using the database obtained from the literature.

4.2.1. Analysis of experimental liquid holdup results

The liquid holdup measurements obtained are shown in Fig. 5 as a function of gas superficial velocities for various values of liquid superficial velocities. This figure clearly shows that an increase in gas superficial velocity induces a decrease in liquid holdup. This is expected since an increase in gas superficial velocity induces an increase in the volume occupied by the gas at the expense of that occupied by the liquid. The opposite behavior is observed when it comes to the increase in

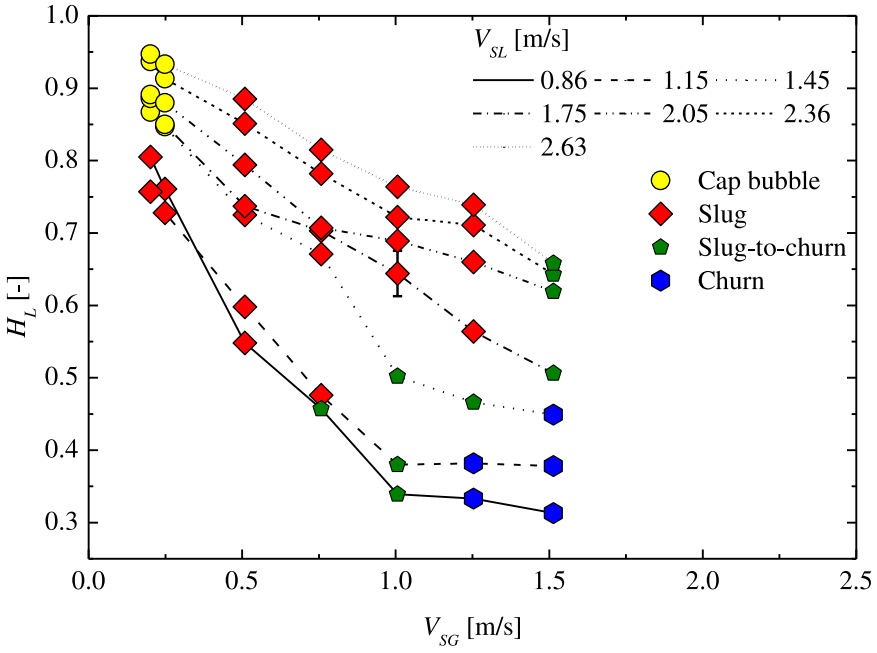

Fig. 5. Evolution of liquid holdup for different operating conditions. Error bar was only put at selected point to improve readability.

liquid superficial velocity. These trends have already been observed in the literature for cap bubble, slug and churn flows (Jiang and Rezakallah, 1993; Xue et al., 2016; Bouyahiaoui et al., 2024). Fig. 5 also shows that the cap-bubble-to-slug flow transition occurs at a value of liquid holdup between 0.85 and 0.88. These values are slightly higher than the critical value of 0.825 reported in Lokanathan and Hibiki (2018). Our experimental results also show that the transition to churn flow occurs at a wide range of H_L (0.47–0.67). The critical value proposed by Lokanathan and Hibiki (2018) (H_L= 0.57) falls within this interval. These results illustrate the general difficulty in associating this flow transition with one critical value of liquid holdup. Similar conclusions can be drawn from measurements obtained by, for example, Xue et al. (2016) and Bouyahiaoui et al. (2024).

For further analysis, the measurements were plotted in Fig. 6a as a function of the liquid-to-gas ratio (V_{SL}/V_{SG}). This figure clearly shows that an increase in the superficial velocities ratio leads to an increase in liquid holdup. Note that the cap bubble data are close to the prediction of the homogenous model, which corresponds to when H_L= λ_L. In this case, both phases flow at the same velocity. The occurrence of slug flow is accompanied by the occurrence of points on each side of the curve. On the other hand, the transition to churn flow induces the transition to a buoyancy dominant flow (i.e., the buoyancy effect is stronger than the inertia), which, mathematically, means that $V_L > V_G$. Note that similar observations can be obtained by analyzing liquid holdup using slip velocity, slip ratio or slippage number or by plotting H_L vs λ_L. To study the effect of V_{SL} on the flow behavior of two-phase vertical downward flow, we have plotted in Fig. 6b the evolution of relative difference between the measured liquid holdup and the input liquid holdup $\left(\frac{H_L-\lambda_L}{H_L}\right)$ as function of V_{SL}. It appears clearly that the buoyancy driven flow behavior decreases with the increase of V_{SL}.

For drift-flux analysis it is common to plot the results of liquid holdup using V_G as a function of V_M. This representation enables the extraction of the distribution parameter and the drift velocity (Ryan et al., 2024). Our experimental results have been plotted using this representation in Fig. 7a and 7b. Different symbols are used for each value of V_{SL} and V_{SG}, respectively. These figures show that all results in the database align themselves linearly. By applying a linear fitting to all data, Eq. (22) was obtained with a coefficient of determination (R^2) equals to 0.9017.

$$V_G = 1.3472V_M - 0.905 \tag{22}$$

However, a considerable deviation around the fit is observed. Fig. 7a shows that the results for each V_{SL} align differently to the line in Eq. (22). For example, the results obtained at V_{SL} equal to 2.63 m/s and 1.15 m/s are situated above and below the fit. The same behavior is observed in relation to V_{SG} in Fig. 7b. We can conclude that the distribution coefficient depends on both V_{SL} and V_{SG}, which may be due to the complex natures of the Taylor bubble shape in vertical downward slug flow (Martin, 1976) (the most dominant flow regime observed in our experiments) and of liquid slug aeration (Saidj et al., 2025). The shape of the Taylor bubble is a result of the influence of the velocity and holdup profiles in both phases and there is therefore a direct relationship between the shape of the Taylor bubble and the distribution coefficient. In Fig. 7c the results are plotted in a similar way to those in Fig. 7a and 7b but differentiated by the nature of the flow regime. This figure shows that the distribution parameter is also influenced by the nature of the flow regime. This result is more clearly observed when we compare the data for churn flow with those for cap bubble and slug flows.

4.2.2. *Development of a new liquid holdup correlation*

Inspired by the recent work of Al-Sarkhi et al. (2024), who correlated the liquid holdup for horizontal, inclined and vertical upward slug flow using the input liquid fraction and liquid-to-gas superficial velocities, we represent our measurements and the data collected from the literature on liquid holdup (summarized in Table 1) using Y_1 as a function of λ_L in Fig. 8. Here, Y_1 is expressed as the ratio between liquid holdup and the liquid-to-gas superficial velocity ratio (Eq. (23)). This figure clearly shows that the vast majority of data collapse in one s-shaped curve. If we bear in mind that these data cover a large range of pipe diameters (1.03 mm ≤ ID ≤ 202.3 mm) and superficial velocities in the two phases and a wide variety of fluids (air-water, N_2-water, air-oil, steam-water, CO_2) and flow regimes, the scatter of the data in Fig. 8 can be considered highly satisfactory, especially for $\lambda_L > 0.75$.

$$Y_1 = \frac{H_L}{V_{SL}/V_{SG}} \tag{23}$$

The trend observed in Fig. 8 can be interpreted as follows. For low values of homogenous liquid holdup, which corresponds to cases where

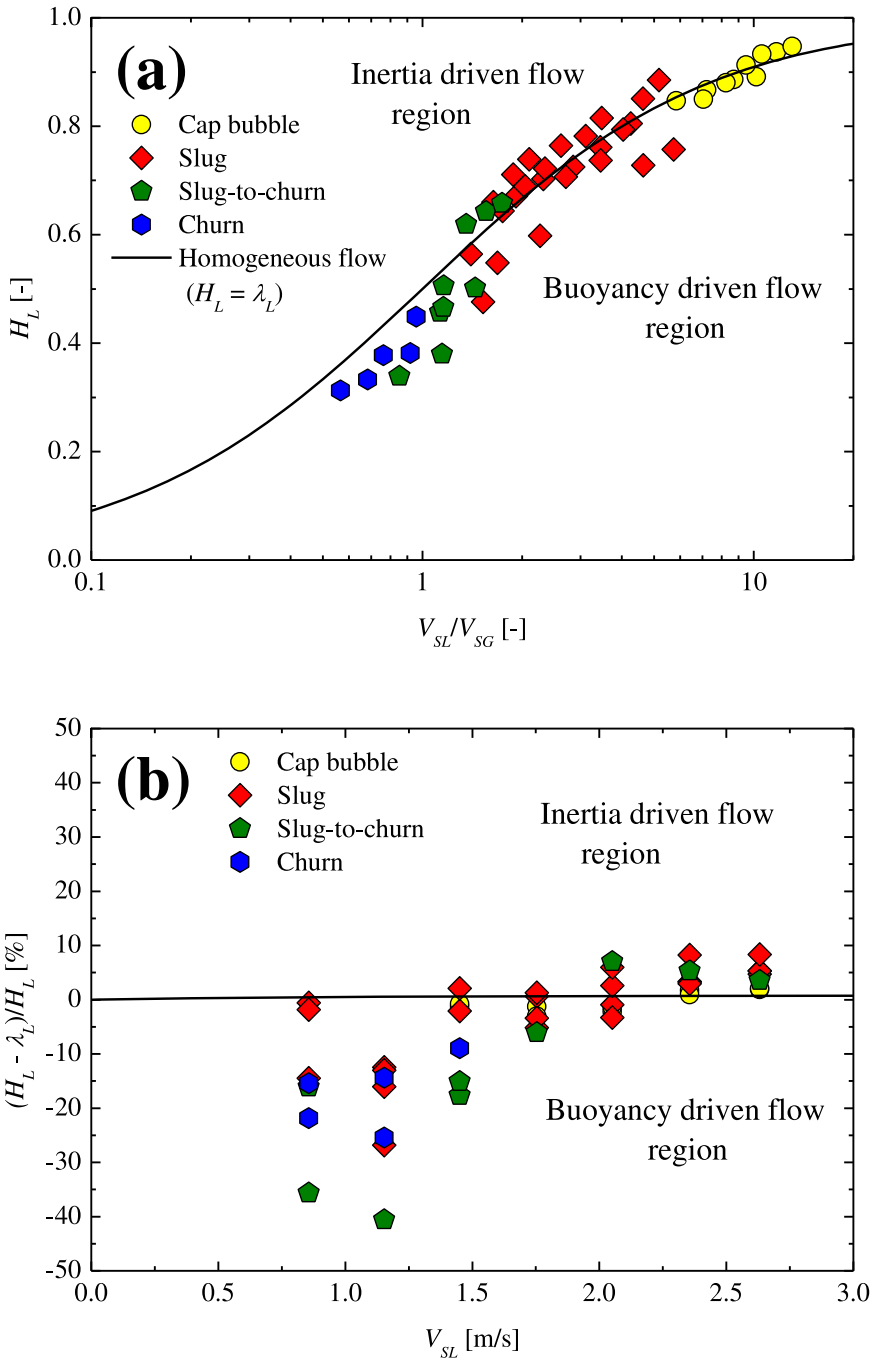

Fig. 6. Evolution of (a) liquid holdup as a function of V_{SL}/V_{SG} and comparison with the homogenous model; and (b) relative difference between liquid holdup and the input liquid holdup as function of V_{SL}.

$V_{SL} << V_{SG}$, Y_1 exhibits relatively large values. An increase in λ_L induces a continuous exponential decrease in Y_1 until it reaches a value of approximately 2, after which it drops linearly and then restarts to exponentially decay from a λ_L value of $\sim$ 0.75. When λ_L approaches unity, which corresponds to cases where $V_{SL} >> V_{SG}$, Y_1 tends towards very low values. These observations for low and high values of input liquid fraction can be explained by disappearance of the effect of gas and liquid superficial velocities in the segregated (falling film and annular) and bubbly flows, which are present in low and high values of λ_L, respectively. This general trend is typical of the inverse function of the sigmoid trend, which can be captured by the logistic function. The logistic function is used in several fields, including biology, medicine, biomathematics, demography, economics, chemistry, statistics, artificial intelligence, signal and image processing (Cioncolini and Thome, 2012; Kyurkchiev and Markov, 2015; Ren and Wang, 2023). In multiphase flow, Cioncolini and Thome (2010) used it to correlate the liquid entrainment in annular flow. In accordance with the work of Jukić and Scitovski (1996) and considering $0 \leq \lambda_L \leq 1$, the following generalized logistic function has been used to correlate λ_L with Y_1:

$$\lambda_L = (1 + b\ exp(caLn(Y_1)))^{-\frac{1}{a}} \tag{24}$$

where c is the growth rate, b is related to the abscissa of maximum growth, and a is the asymmetry coefficient.

In Fig. 9, the 457 data points from our experiments and those by Ishii et al. (2004), Vieira et al. (2015), Olarinoye (2021) and Shi et al. (2021)

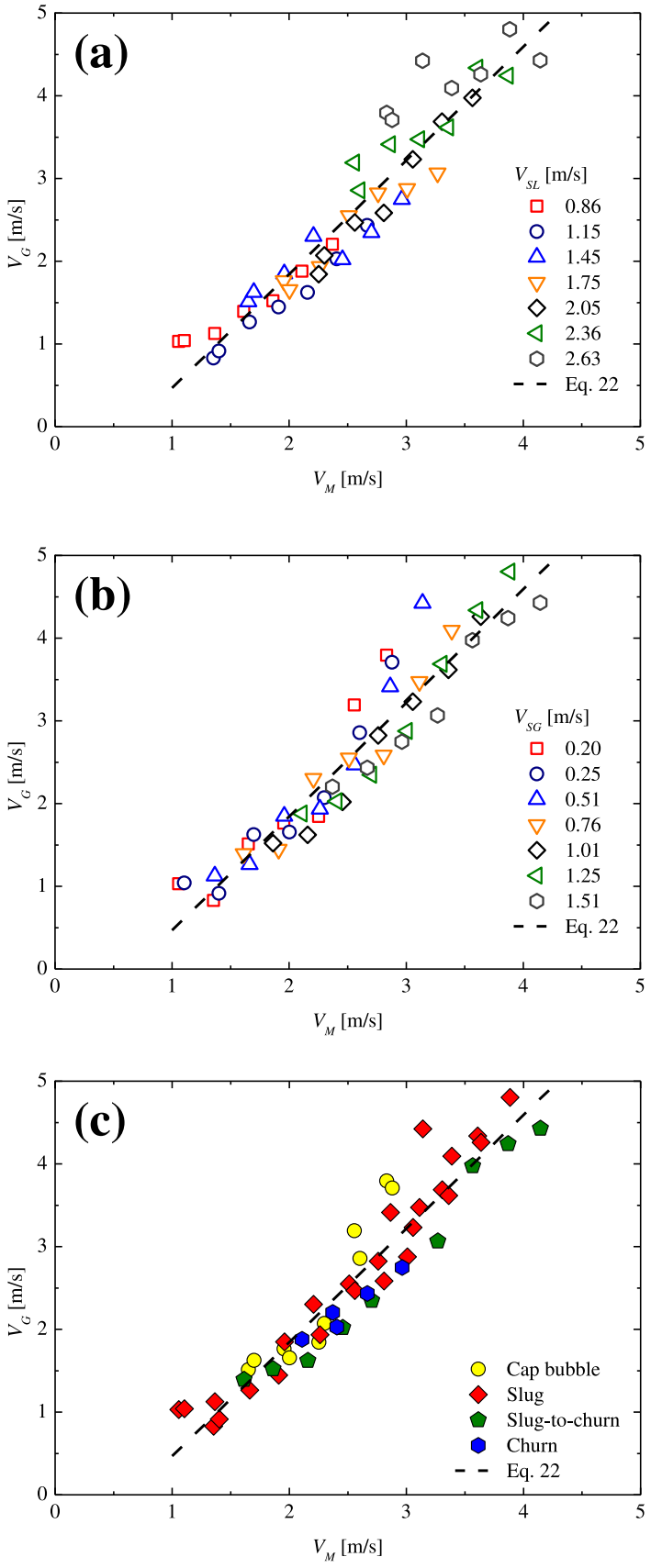

Fig. 7. Plot of liquid holdup measurements using the V_G vs V_M plot and taking into account (a) V_{SL} values, (b) V_{SG} values, and (c) the nature of the flow regime.

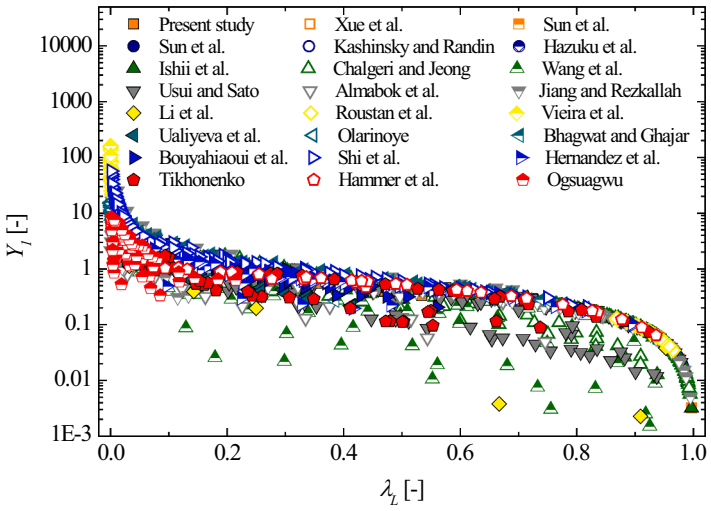

Fig. 8. Plot of the present results and those collected from the literature using Y_1 vs λ_L.

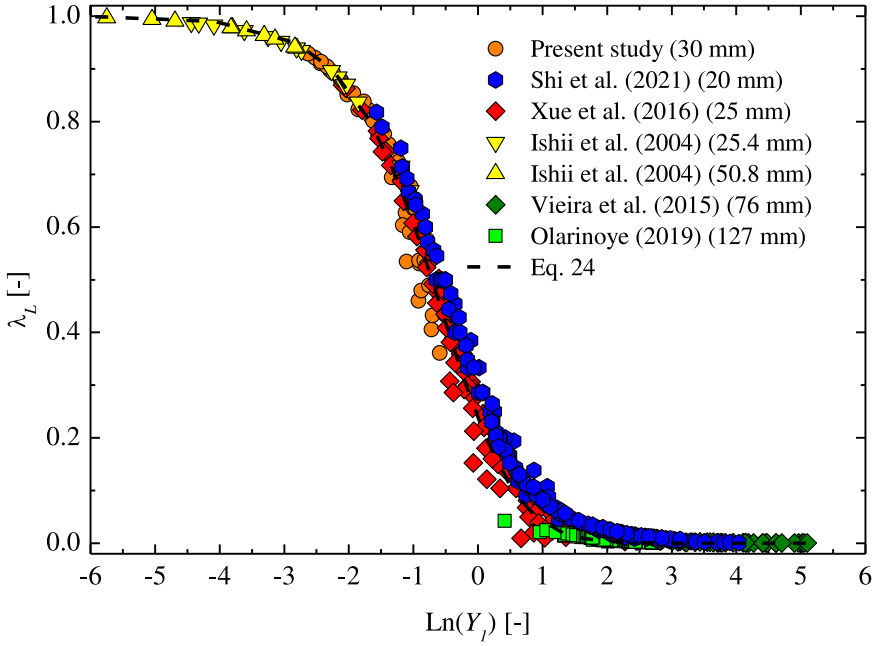

Fig. 9. Plot of selected data for developing the liquid holdup model using λ_L vs Ln(Y_1).

are plotted using λ_L vs Ln(Y_1) to develop a model. This database was chosen because the data cover a wide range of input liquid fractions ($0.0002 \leq \lambda_L \leq 0.9968$) and pipe diameters (20 mm to 127 mm) as well as a wide range of flow regimes (bubbly, cap bubble, slug, churn, annular and falling film). As we discuss in Section 4.2.3, the remaining data from the collected database were used for validation purposes. By using MATLAB's curve fitting toolbox, parameters *b, c* and *a* were found to be 1, 2.7211 and 0.4804, respectively, while the coefficient of determination (R^2) was 0.9946. The relation between Y_1 and λ_L can therefore be written as:

$$Y_1 = \left(\lambda_L^{-0.4804} - 1\right)^{0.765} \tag{25}$$

The final correlation of liquid holdup is therefore:

$$H_L = \frac{V_{SL}}{V_{SG}}\left(\lambda_L^{-0.4804} - 1\right)^{0.765} \tag{26}$$

Note that when λ_L tends to 1, Eq. (26) give values that are equal or greater than 1. Since this range corresponds to bubbly flow, which exhibits homogenous behavior (Roustan et al., 1992), the following condition was added:

$$H_L = \lambda_L \text{ if } H_L \geq 1 \tag{27}$$

4.2.3. *Evaluation of the existing and proposed liquid holdup models*

The liquid holdup models reported in the literature (listed in Table 2) and the model proposed in Eqs. (26) and (27) were evaluated by comparing the predictions calculated with the experimental data made up of 1646 points. This enabled us to note that if $V_{SG} > C_0V_M\text{-}V_{gd}$ and $C_0V_M\text{-}V_{gd} < 0$, H_L values given by the drift-flux based models are smaller than 0 or larger than 1, respectively, which is physically impossible. This case occurs only at low liquid and gas superficial velocities, which generally correspond to falling film flow conditions. The occurrence of the this case is possible because V_{gd} is negative for vertical downward flow. However, this is not the case for vertical upward or horizontal flows, where V_{gd} attains positive and zero values, respectively (Rassame and Hibiki, 2018; Dong et al., 2020). Note that all evaluated drift-flux

Table 5
Evaluation of the liquid holdup predictive models.

Datasource	Yamazaki and Yamaguchi (1979)	Dong and Hibiki (2021)	Developed correlation
Tikhonenko (1973) (33 mm ID) (P= 1.96 MPa)	172.81	35.86[a]	123.76
Tikhonenko (1973) (33 mm ID) (P = 9.06 MPa)	109.64	12.17[b]	72.01
Usui and Sato (1989) (16 mm ID)	108.10	34.19[c]	100.89
Usui and Sato (1989) (24 mm ID)	89.70	29.22[d]	80.33
Roustan et al. (1992) (50 mm ID)	1.04	0.97	2.75
Jiang and Rezkallah (1993) (9.53 mm ID)	86.39	45.39[e]	49.50
Kashinsky and Randin (1999) (42.3 mm ID)	0.95	4.27	2.13
Hernandez et al. (2002) (50.8 mm ID)	57.47	18.38[f]	27.25
Sun et al. (2004a) (50.8 mm ID)	1.62	1.48	0.95
Sun et al. (2004b) (50.8 mm ID)	2.17	2.44	1.75
Ishii et al. (2004) (25.4 mm ID)	2.28	2.56	2.51
Ishii et al. (2004) (50.8 mm ID)	1.33	1.34	0.51
Bhagwat and Ghajar (2012, 2017) (12.7 mm ID)	17.29	45.99[g]	32.57
Vieira et al. (2015) (76 mm ID) (μ_L= 1 cP)	31.13	94.78[h]	66.43
Vieira et al. (2015) (76 mm ID) (μ_L= 10 cP)	42.91	96.05[i]	75.90
Almabrok et al. (2016) (101.6 mm ID)	157.78	43.68[j]	94.35
Xue et al. (2016) (25 mm ID)	27.38	17.31	12.71
Wang et al. (2018) (203.2 mm ID)	980.08	365.71[k]	886.71
Li et al. (2018) (203.2 mm ID)	2296.09	826.33[l]	2165.70
Chalgeri and Jeong (2019) (D_h= 4.55 mm)	28.19	11.39	22.51
Hazuku et al. (2020) (1.03 mm ID)	1.52	5.10[m]	1.36
Hazuku et al. (2020) (3 mm ID)	1.24	3.31	0.41
Hazuku et al. (2020) (5 mm ID)	1.48	3.68	0.60
Bouyahiaoui et al. (2020) (34 mm ID)	46.2	14.82	29.72
Shi et al. (2021) (20 mm ID)	19.61	54.62[n]	40.09
Olarinoye (2021) (127 mm ID)	61.96	82.65[o]	20.62
Hammer et al. (2021) (44 mm ID)	32.72	-*	19.62
Ualiyeva et al. (2022) (50.8 mm ID) (μ_L= 4 cP)	92.41	50.49	61.11
Ualiyeva et al. (2022) (50.8 mm ID) (μ_L= 7 cP)	108.83	63.52	74.99
Osuagwu (2024) (50.8 mm ID)	197.76	63.58[p]	88.25
Present study (30 mm ID)	11.16	7.13	10.21

*the predictions given by the model of Dong and Hibiki (2021) were not calculated since the physical properties of CO_2 are not available.
[a] 1 datum on a total of 33 gave unphysical predictions.
[b] 2 data on a total of 24 gave unphysical predictions.
[c] 12 data on a total of 55 gave unphysical predictions.
[d] 10 data on a total of 106 gave unphysical predictions.
[e] 11 data on a total of 95 gave unphysical predictions.
[f] 8 data on a total of 91 gave unphysical predictions.
[g] 1 datum on a total of 95 gave unphysical predictions.
[h] 19 data on a total of 24 gave unphysical predictions.
[i] 16 data on a total of 19 gave unphysical predictions.
[j] 10 data on a total of 67 gave unphysical predictions.
[k] 4 data on a total of 56 gave unphysical predictions.
[l] 1 datum on a total of 6 gave unphysical prediction.
[m] 1 datum on a total of 3 gave unphysical prediction.
[n] 3 data on a total of 167 gave unphysical predictions.
[o] 35 data on a total of 86 gave unphysical predictions.
[p] 15 data on a total of 75 gave unphysical predictions.

models exhibit some points where the above condition is met.

To compare performance, the average absolute relative error (*AARE*) (given by Eq. (28)), based on the relative error between the measured and the calculated liquid holdup (*RE*) (given by Eq. (29)), is used to quantitatively analyze the prediction levels of the evaluated models.

$$AARE = \frac{1}{N}\sum_{i=1}^{N}|RE| \tag{28}$$

$$RE = \frac{PV_{exp} - PV_{cal}}{PV_{exp}} \tag{29}$$

where N and PV refer to the number of data points and the physical parameter (which in this case is liquid holdup), respectively. Subscripts *cal* and *exp* stand for the calculated and experimental values, respectively.

The summary of *AAREs* for models of Yamazaki and Yamaguchi (1979), Dong and Hibiki (2021) and the proposed ones are shown in Table 5. Note that based on conclusions reported in relation to drift-flux models, we choose to assess only the drift-flux model of Dong and Hibiki (2021) which has the highest range of applicability. The statistical performances of the other drift-flux models are shown in Appendix B. If we analyze Table 5, it appears that the prediction of each model depends on the dataset considered (note that this is also valid for the other drift-flux models). The present correlation provides good predictions, with $AARE \leq 25$ %, and performs better than the two other models with great numbers of datasets, including those of Sun et al. (2004a, 2004b), and Hazuku et al. (2020), which were not used for its development. It also provides the best predictions for the data of Hammer et al. (2021), which were obtained with CO_2. As a future work, it will be interesting to assess the range of applicability of each model for different range of pipe diameter and operating conditions.

Fig. 10 plots the predictions made by the proposed model with the present datasets. Most of the data are predicted with a confidence range of ±20 %, which can be considered satisfactory. This figure also shows that the nature of the flow regime influences the performance of the model. As we see in Appendix B, this statement is valid for all evaluated models.

4.3. Single-phase pressure drop and choice of friction factor model

As reported by Li and Chen (2024), the accuracy of single-phase frictional pressure drop forms the basis for two-phase flow pressure drop measurements. Based on this principle, for validation purposes we conducted experimental measurements of liquid single-phase pressure drop for the two-phase flow pressure drop data. The static pressure profiles obtained using the four pressure transducers for different values of V_L are illustrated in Fig 11. The decrease in pressure with height is due to the greater contribution from gravitational pressure drop compared to that from frictional pressure drop. Note also that these profiles are almost perfectly linear. The slight deviation observed in some cases is due to the measurement collected at the first point. This means that the flow is fully developed from the second measurement point located at a distance of 56.33D from the end of the bend. Based on this observation, we considered only the pressure profiles obtained at points 2, 3 and 4 to determine the total pressure drop slope.

The liquid single-phase frictional pressure drop measurements were calculated by subtracting the total pressure drop from the calculated single-phase flow gravitational pressure drop. The single-phase frictional pressure drops obtained are plotted in Fig. 12a using the friction factor (calculated from Eq. (6)) as a function of the Reynolds number. The curves provided by existing friction factor models, which are summarized in Table 6, are also shown. Fig. 12a clearly shows that all the models provide accurate predictions. With a satisfactory average relative error of 2.69 %, the best performances were obtained using Fang et al.'s (2011) model. As Fig. 12b shows, only one datum was predicted in the greater than ±5 % range. Based on this observation, Fang et al.'s

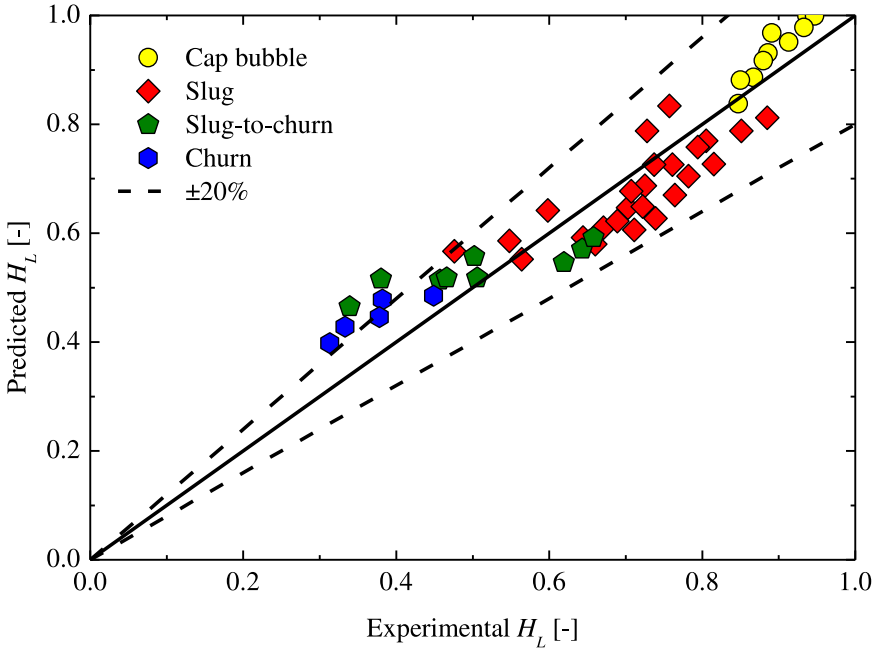

Fig. 10. Experimental liquid holdup results compared with predictions provided by the proposed model.

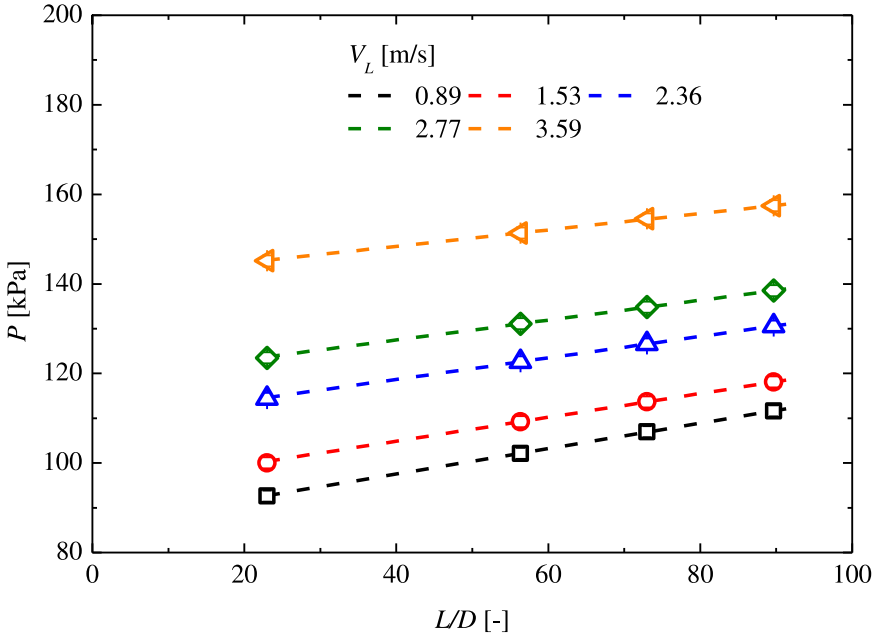

Fig. 11. Local liquid single-phase flow pressure along the test section for different liquid velocities. Single phase total pressure drop profile.

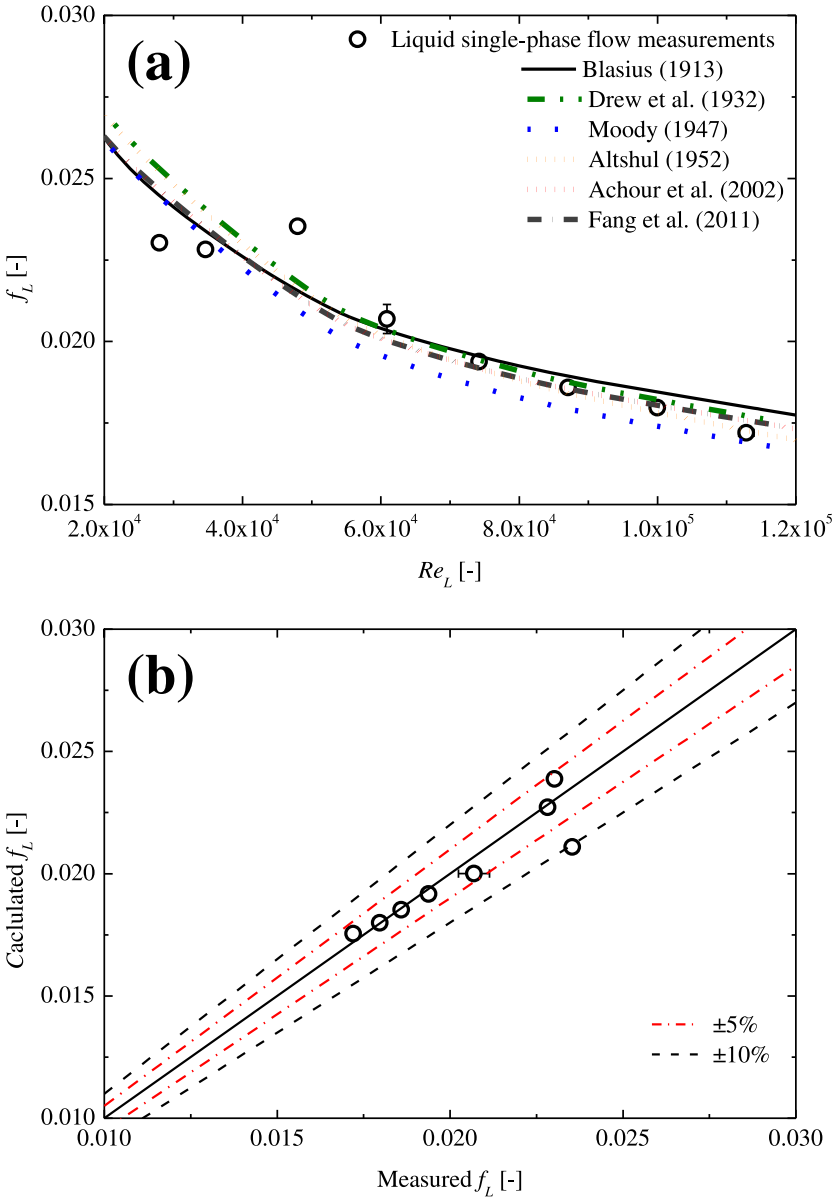

Fig. 12. . (a) Evolution of the measured liquid single-phase friction factor results as a function of the Reynolds number and comparison with existing models; and (b) experimental friction factor results compared to the prediction provided by Fang et al.'s (2011) model. Error bar was only put at selected point to improve readability.

Table 6
Summary of friction factor models evaluated in this study.

Authors and year	Correlation
Blasius (1913)	$f = \begin{cases} 0.316Re^{0.25} \text{ if } Re \leq 2 \times 10^4 \\ 0.184Re^{0.25} \text{ if } 2 \times 10^4 \leq Re \leq 2 \times 10^6 \end{cases}$
Drew et al. (1932)	$f = 0.0056 + \frac{0.5}{Re^{0.32}}$
Moody (1947)	$f = 0.0055\left[1 + \left(2 \times 10^4 \frac{\varepsilon}{D} + \frac{10^6}{Re}\right)^{1/3}\right]$
Altshul (1952)*	$f = 0.11\left(\frac{\varepsilon}{D} + \frac{68}{Re}\right)^{0.25}$
Achour et al. (2002)	$f = \left[-2log\left(\frac{\varepsilon/D}{3.7} + \frac{4.5}{Re} log\left(\frac{Re}{6.97}\right)\right)\right]^{-2}$
Fang et al. (2011)	$f = 0.25\left[log\left(\frac{150.39}{Re^{0.98865}} - \frac{152.66}{Re}\right)\right]^{-2}$

* cited by Genić et al. (2011).

(2011) model was considered in this study.

In this paper we also took into account that the laminar-to-turbulent transition occurs at Re= 1055. As shown recently by Bouyahiaoui et al. (2024), this value corresponds to the intersection of the laminar and turbulent friction factor curves. Interestingly, Friedel (1979) used the same value for the critical Reynolds number.

4.4. Total pressure drop

In this section we discuss the profiles of total pressure drop for two-phase flow. The effect of V_{SL}, V_{SG} and flow regime will be analyzed with special emphasis on the dimensionless number based on the total pressure drop proposed by Bouyahiaoui et al. (2020).

4.4.1. Two-phase static pressure drop profiles

As with single-phase flow (Section 4.3), Fig. 13 shows the two-phase pressure profiles obtained using the four pressure transducers for nine

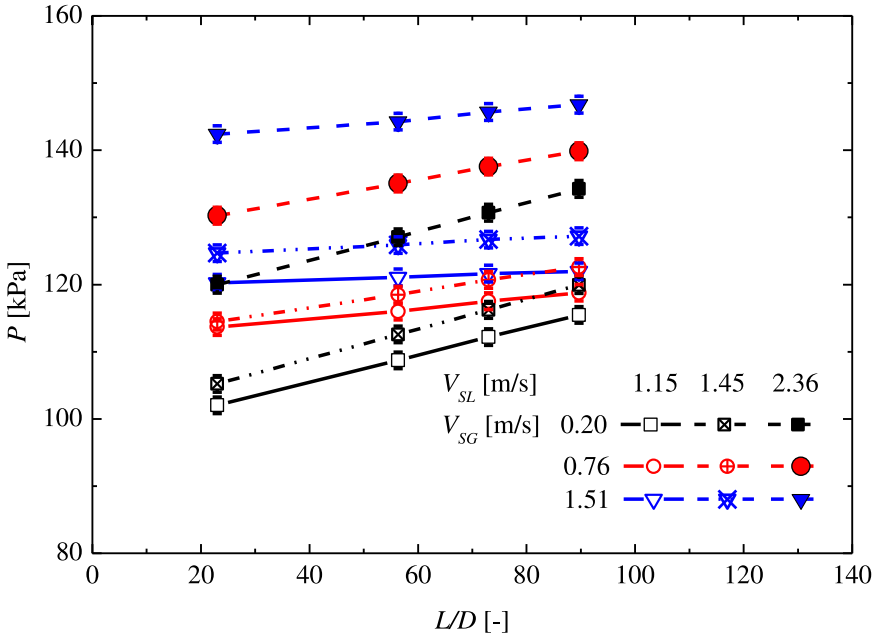

Fig. 13. Local two-phase flow pressure along the test section for different liquid and gas superficial velocities.

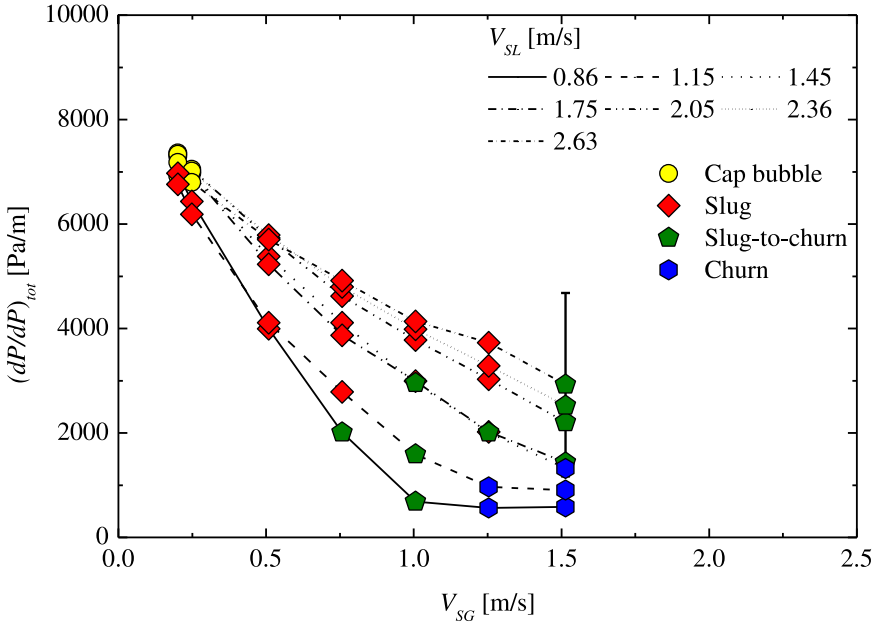

Fig. 14. Evolution of total pressure drop for different operating conditions. Error bar was only put at selected point to improve readability.

conditions corresponding to V_{SL}= 1.15 m/s, 1.45 m/s and 2.36 m/s and V_{SG}= 0.2 m/s, 0.76 m/s and 1.51 m/s. This figure clearly shows that the pressure profiles exhibit a linear trend. On the other hand, an increase in both V_{SL} and V_{SG} induced an increase in the measured absolute pressure. The same behavior has already been reported in experiments by Mena (2016) and Qiao and Kim (2018). As with liquid single-phase flow, the flow was fully developed at L/D = 56.33. We therefore considered the last three measurement locations to extract the total two-phase flow pressure drop. Note that Lau and Rezkallah (1995) stated that the effect of the entrance effect in vertical downward flow is insignificant after 52 L/*D*.

4.4.2. Analysis of total pressure drop results

The total pressure drop measurements are shown in Fig. 14 as a function of V_{SG}. Different symbols were used for each flow regime. Note that an increase in V_{SG} induces a decrease in total pressure drop. This trend increases with the transition to slug flow. This is because the total pressure is mainly impacted by the gravitational pressure drop, which is inversely proportional to the gas flow rate. With the transition to churn flow, the total pressure drop becomes almost constant. On the other hand, as Fig. 14 shows, total pressure drop is positively impacted by V_{SL}. One also note that the measured two-phase flow total pressure drops are lower than the liquid-single phase gravitational pressure drop (which is approximatively equal to 9780 Pa/m). These findings further support the dominance of the gravitational pressure drop over the frictional pressure drop.

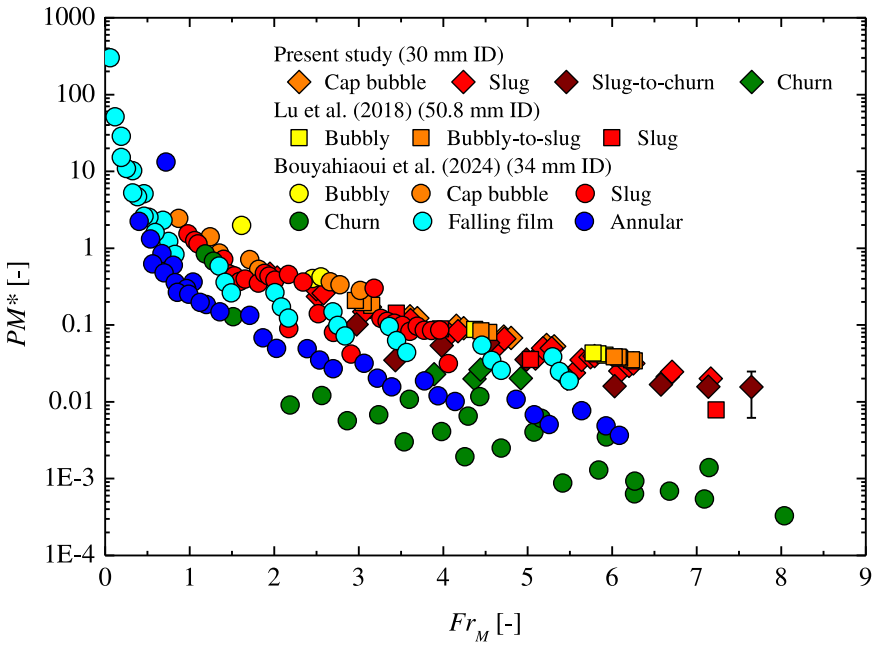

Fig. 15. Experimental results and those of Lu et al. (2018) and Bouyahiaoui et al. (2024) using PM^* vs Fr_M. Error bar was only put at selected point to improve readability.

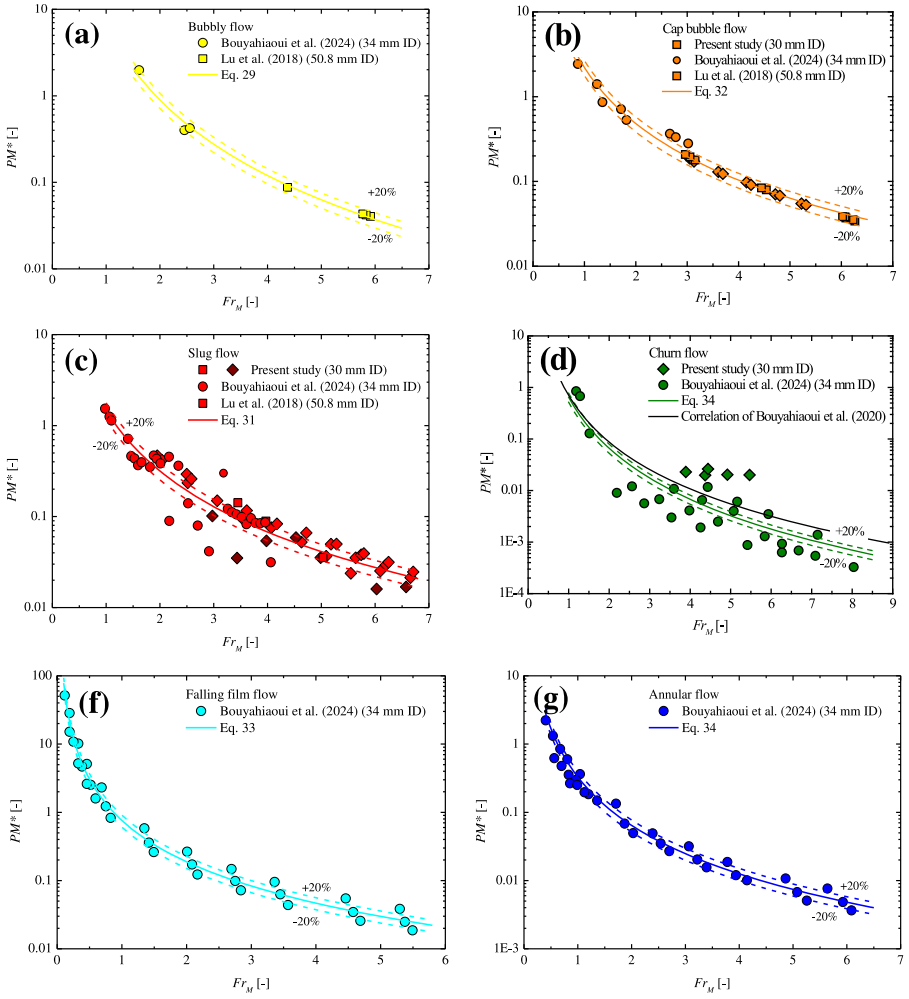

Fig. 16. Plot of all the experimental results and those of Lu et al. (2018) and Bouyahiaoui et al. (2024) using PM^* vs Fr_M by differentiating the nature of the flow regime: (a) bubbly, (b) cap bubble, (c) slug, (d) churn, (e) falling film, and (f) annular flows.

4.4.3. Dimensionless total pressure drop

Bouyahiaoui et al. (2020) showed that the dimensionless form of the total pressure drop (PM^*) can be correlated with the mixture Froude number (Fr_M) by means of Eq. (30). Note that the above study was conducted only with churn flow.

$$PM^* = 0.7049 Fr_M^{-3.018} \tag{30}$$

Parameters PM^* and Fr_M are calculated using Eqs. (31) and (32), respectively.

$$PM^* = \frac{D(dP/dL)_{tot}}{\frac{1}{2}\rho_{TP} V_M^2} \tag{31}$$

$$Fr_M = \sqrt{\frac{\rho_L}{\rho_L - \rho_G}} \frac{V_M}{\sqrt{gD}} \tag{32}$$

In Fig. 15 our experimental results and those obtained by Lu et al. (2018) and Bouyahiaoui et al. (2024) were plotted using the two dimensionless numbers from the above study. This figure shows that although they align themselves separately, the data from each flow regime follow the same trend. This correlation includes relevant physical parameters such as liquid and gas densities, mixture velocity, and gravitational acceleration, which were already explained in our discussion of Fig. 14.

By considering power law fitting for each flow regime (Fig. 16), the correlations for bubbly, cap bubble, slug, churn, falling film and annular flows, respectively, are given by Eqs. (33)–(38), respectively. The coefficients of determination were 0.9899, 0.9816, 0.9463, 0.9352, 0.9915 and 0.0926, respectively.

$$PM^* = 6.6494 Fr_M^{-2.896} \tag{33}$$

$$PM^* = 2.2172 Fr_M^{-2.208} \tag{34}$$

$$PM^* = 1.4775 Fr_M^{-2.224} \tag{35}$$

$$PM^* = 0.6438 Fr_M^{-3.286} \tag{36}$$

$$PM^* = 0.7591 Fr_M^{-2.012} \tag{37}$$

$$PM^* = 0.3293 Fr_M^{-2.357} \tag{38}$$

Note that the data for slug-to-churn flow transition in this study and the bubbly-to-slug flow transition of Lu et al. (2018) were grouped with the data of slug and cap bubble flows, respectively. Fig. 16 shows that for bubbly, cap bubble and annular flow, most points are predicted within the ± 20 % range. On the other hand, the fit for churn flow is close to that proposed by Bouyahiaoui et al. (2020) for low values of Fr_M.

4.5. Frictional pressure drop

As previously discussed in Section 2, the frictional pressure drop is obtained by subtracting the gravitational pressure drop, calculated using the measured liquid holdup, from the experimentally measured total pressure drop. In this section, we first analyze the calculated frictional pressure drop values obtained from our experiments. Subsequently, a new empirical correlation is proposed based on the analyzed data. Finally, the performance of the proposed correlation is evaluated and compared with existing models using both our dataset and relevant data available in the open literature.

4.5.1. Analysis of experimental frictional pressure drop results

In Fig. 17, we plot the calculated frictional pressure drop as a function of V_{SG}. This figure shows that increases in both V_{SL} and V_{SG} induced a general increase in frictional pressure drop. This result was expected since, as was explained in Section 2, the two-phase frictional pressure drop is made up of liquid and gas frictional pressure drop. Despite the general increase in frictional pressure drop as V_{SG} increases, some decreasing trends can be observed in slug flow. One example is that of V_{SL}= 1.45 m/s and 0.76 m/s $\leq V_{SG} \leq$ 1.25 m/s. Similar behavior was reported in the studies by Yao et al. (2018) and Bouyahiaoui et al. (2024). This observation, which has not been reported for horizontal or vertical upward slug flow, is another example of the specificity of intermittent flow for this pipe orientation. This behavior may be related to the complex nature of the liquid slug aeration mechanism recently discussed by Saidj et al. (2025).

The Lockhart-Martinelli approach is a tool for analyzing frictional pressure drop measurements (Muzychka and Awad, 2010; Lu et al., 2018; Sassi et al., 2020a; Höhn et al., 2025b). It involves representing the data using Φ_L as a function of X. In Fig. 18a our results are depicted using this method. Lines representing Chisholm parameter values of 5, 10, 12, 20, 25, 50, 100 and 652 are also displayed: these correspond to

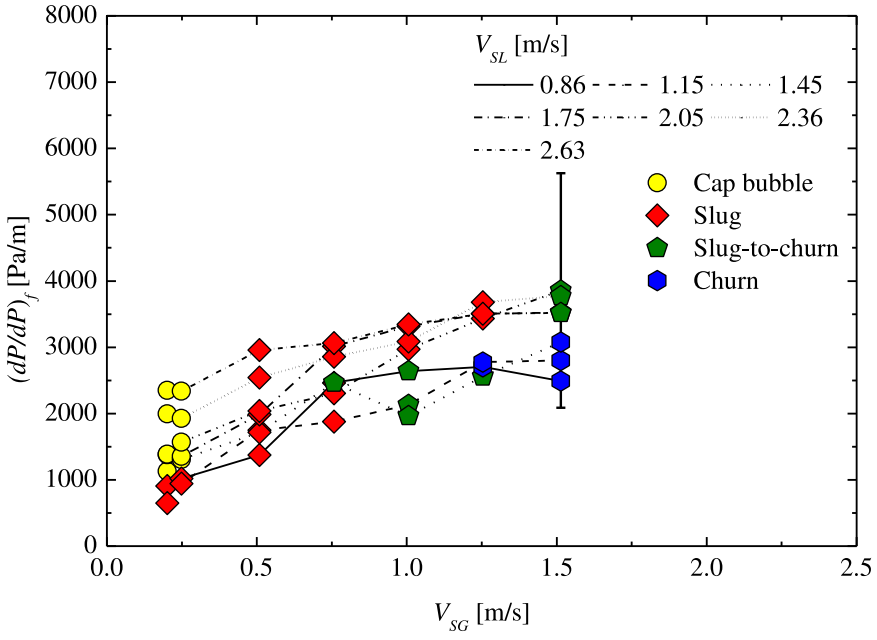

Fig. 17. Evolution of total pressure drop for different operating conditions. Error bar was only put at selected point to improve readability.

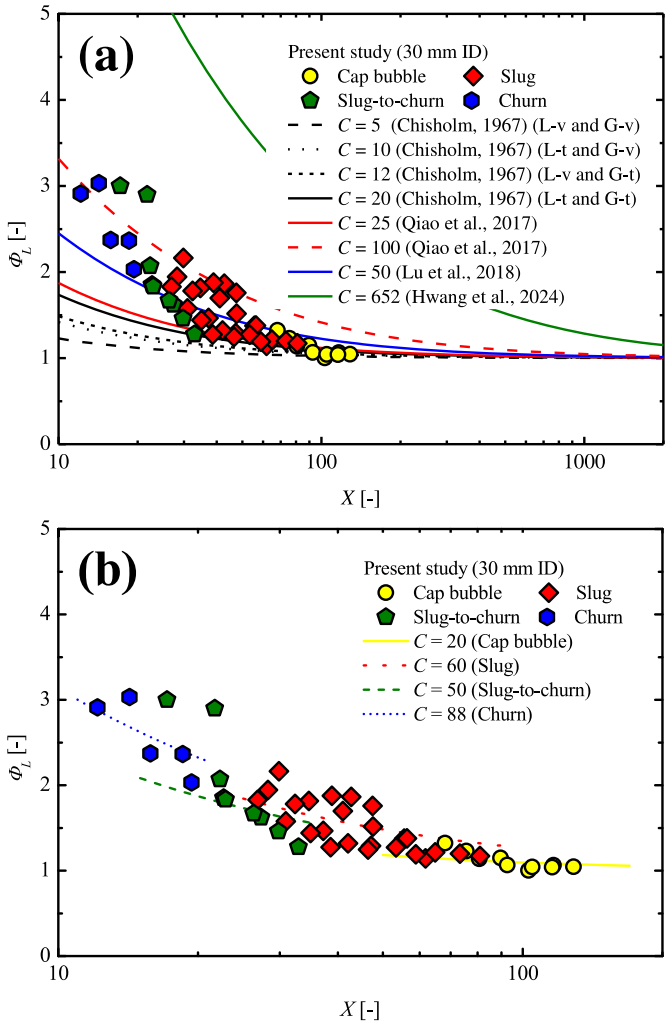

Fig. 18. Plot of the frictional pressure drop measurements obtained in this study using Φ_L vs X and the C value curves (a) proposed by several authors; and (b) obtained by fitting the data of each flow regime separately.

values proposed by several authors (see Table 4). Note that:

1. None of the C values can satisfactorily predict all the experimental results. Correlating the two-phase flow multiplier with only one value of C therefore seems inadequate because of the complex behavior of the vertical downward frictional pressure drop. This behavior is easily observed with the slug and churn flows. The same finding was recently reported by Höhn et al. (2025b) for vertical upward flow.
2. The points collected for each flow regime behave differently.

The latter observation can be quantified by fitting the dataset for each flow regime using the functional form of Eq. (16). The obtained optimal values of C for the cap bubbly, slug, slug-to-churn and churn flows are 20, 60, 50, and 88, respectively; while the corresponding coefficients of determination are 0.3858, 0.4144, 0.8668, and 0.5259, respectively. These values were depicted in Fig. 18b where one can observe an existence of important deviation of the data around the C curves. This shows the difficulty to associate one value for each flow regime.

The results of frictional pressure drop can also be analyzed from the plot of Φ_L vs H_L depicted in Fig. 19. In the literature, several authors correlated the two parameters using Eq. (39). For instance, Lu et al. (2018), Yamazaki and Yamaguchi (1979) and Lau and Rezakallah (1995) reported optimum exponent n values of 0.875, 0.9 and 1.14, respectively. One can see from Fig. 19 that the two former values match better with the present data.

$$\Phi_L = H_L^{-n} \tag{39}$$

4.5.2. Development of a new frictional pressure drop correlation

Further analysis of Fig. 18a shows that the values of the Chisholm parameter proposed by Chisholm (1967) tend to underpredict the frictional pressure drop for all these datasets. This confirms that an additional term (B) must be added to the Chisholm formulation. According to Yao et al. (2018), this term is due to the buoyancy force which acts in the opposite direction to the flow and creates additional friction. As explained in our discussion on flow regimes presented in Section 4.1, cap bubble and churn flows can be considered slug flow. In slug flow, Taylor bubble can be seen as elongated bubble flowing on a continuous liquid, as shown in in Fig. 20. The buoyancy force (F_b) acting on the Taylor bubble can be calculated as:

$$F_b = (\rho_L - \rho_G) g\ Vol \tag{40}$$

where Vol is the volume of the displaced fluid, which is equal to the volume of the Taylor bubble. If we assume that a Taylor bubble is a perfect cylinder, its volume can be calculated from Eq. (41).

$$Vol = \Pi \frac{D_{TB}^2}{4} L_{TB} \tag{41}$$

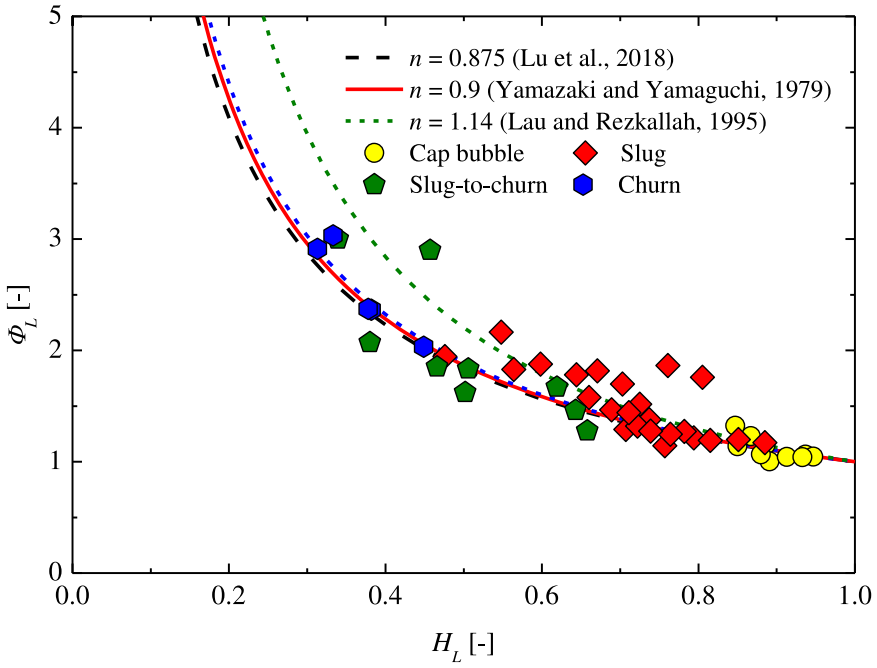

Fig. 19. Experimental frictional pressure drop results using Φ_L vs H_L and comparison with various correlations.

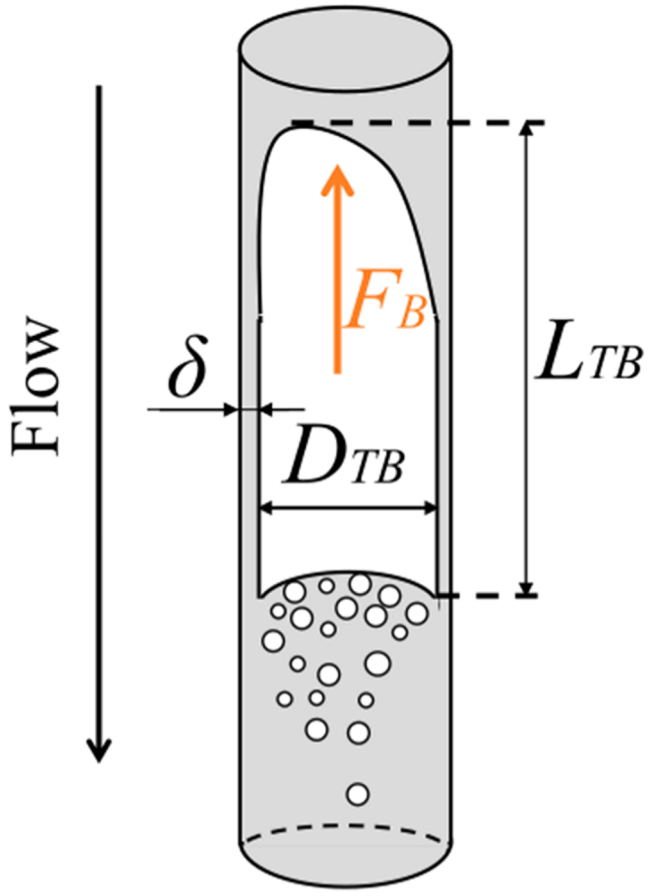

Fig. 20. Schematic diagram of a Taylor bubble in gas-liquid vertical downward flow.

where L_{Tb} and D_{TB} refer to the length and diameter of a Taylor bubble.

Fewer studies have measured the dimensions of Taylor bubbles in vertical downward flow than in vertical upward flow. One study, however, is that by Bouyahiaoui et al. (2018), which was conducted with a 34 mm ID pipe and an air-water mixture. Using their database on Taylor bubble length and diameter (computed from the liquid film thickness (δ)), the Taylor bubble volume can be correlated with the Lockhart–Martinelli parameter by means of parameter Y (Eq. (42)). Visualizing the results obtained by Bouyahiaoui et al. (2018) using the log-scale produces the linear fit shown in Fig. 21.

$$Y = \frac{Vol f_L}{Vol_{ref} \lambda_L f_G} \tag{42}$$

Note that Vol_{ref} in Eq. (42) was taken equal to 1 m^3.

Intuitively we can guess that the fourth term of the two-phase flow multiplier is proportional to the buoyancy force and, therefore, to the volume of the Taylor bubble (Eq. (43)).

$$B \propto F_b \propto Vol \tag{43}$$

Based on Eq. (43) and the finding highlighted in Fig. 21, we expect B to be correlated with X through Y_2, which, as Eq. (44) shows, is copied on Y. To confirm this assumption, we present the calculated B values for the database on frictional pressure drop (our measurements and the datasets listed in Table 3) using $\mathrm{Ln}(Y_2)$ as a function of $\mathrm{Ln}(X)$. Note that the calculated B values were obtained by subtracting the two-phase multiplier provided by Chisholm's (1967) model from the two-phase multiplier calculated from the experimental measurements. These plots exhibit the same tendencies as those reported in Fig. 21 with most datasets. An example is provided in Fig. 22, which combines our data with those of Lau and Razkallah (1995) and Almabrok (2013), which will be used to develop the model. Note that, as reported in relation to the Taylor bubble volume measurements, the data from these authors exhibit a linear tendency. As shown in Table 3, the datasets of Lau and Razkallah (1995) and Almabrok (2013) contain different flow regimes, including segregated and bubbly flows. This means that all flow regimes followed the same trend as slug flow, which, from the physical analysis performed, was not expected.

$$Y_2 = \frac{B f_L}{\lambda_L f_G} \tag{44}$$

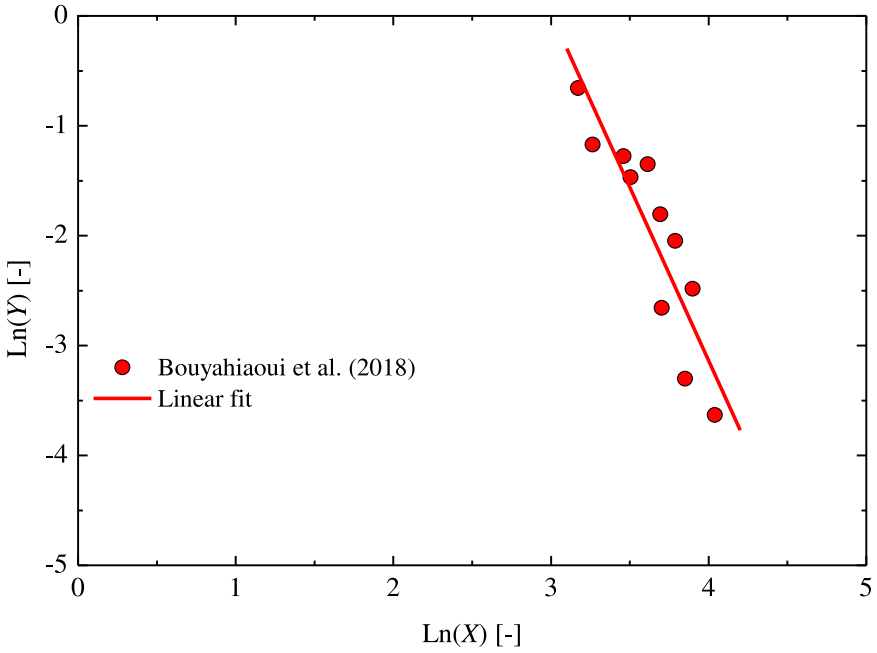

Fig. 21. Taylor bubble volume measurements obtained by Bouyahiaoui et al. (2018) using Ln(Y) vs Ln(X).

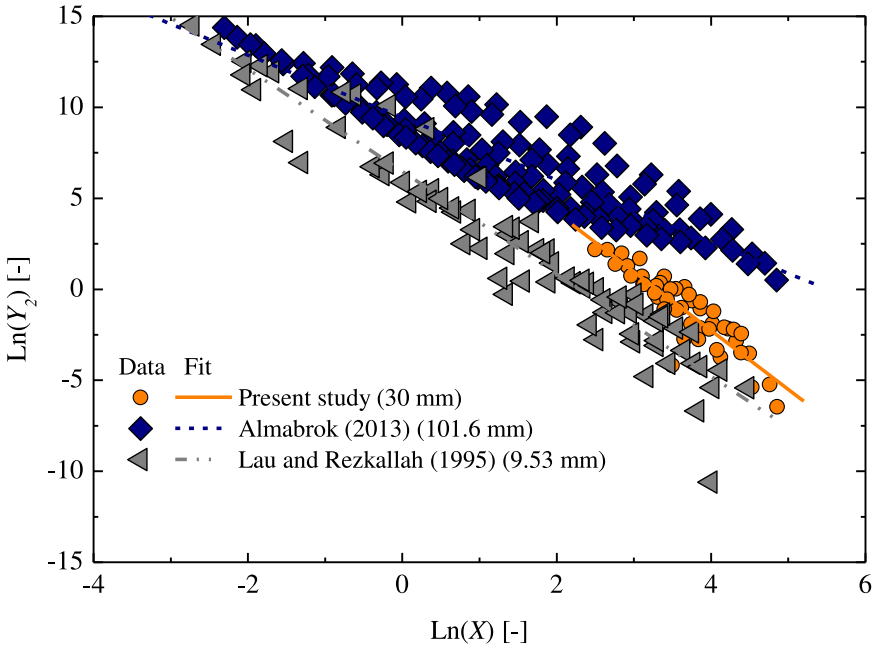

Fig. 22. Selected data for developing the frictional pressure drop model using Ln(Y_2) vs Ln(X).

By fitting the data from each database separately, we observed that the intercept was almost constant and equal to 8.8609, while the slope was linearly correlated with the pipe diameter. Based on these results, Ln(Y_2) and Ln(X) were correlated as follows:

$$Ln(Y_2) = (13.743D - 3.2537)Ln(X) + 8.8609 \quad (45)$$

From the previous correlation, B is given as:

$$B = \frac{f_G \lambda_L \exp\left[(13.743D - 3.2537)Ln(X) + 8.8609\right]}{f_L} \quad (46)$$

Finally, the proposed model holds as:

$$\Phi_L^2 = 1 + \frac{C}{X} + \frac{1}{X^2} + \frac{f_G \lambda_L \exp\left[(13.743D - 3.2537)Ln(X) + 8.8609\right]}{f_L} \quad (47)$$

where C is calculated using Chisholm's (1967) correlation (Eq. (17)).

4.5.3. Evaluation of the existing and the proposed frictional pressure models

As with liquid holdup, we assessed the correlation developed in this paper and those currently available in the literature (listed in Table 4) with our experimental measurements and those collected from the literature (listed in Table 3) made up of 714 data points. The calculated *AARE* are summarized in Table 7. Note that the negative values for the frictional pressure drop gradient of the data from Bouyahiaoui et al.

Table 7
Evaluation of the frictional pressure drop predictive models.

Datasource	Yamazaki and Yamaguchi (1979)	Friedel (1979)	Lau and Rekallah (1995) Annular flow	Qiao et al. (2017) (C = 25)	Qiao et al. (2017) (C = 100)	Yao et al. (2018)	Lu et al. (2018)	Hwang et al. (2024)	Developed correlation
Roustan et al. (1992) (50 mm ID)	33.39	35.8	94.58	34.23	63.34	29.03	42.91	430.55	37.8
Lau and Rezkallah (1995) (9.53 mm ID)	30.81	50.77	63.26	26.36	171.97	43.14	65.12	1394.85	231.78
Sun et al. (2004a) (50.8 mm ID)	30.18	28.12	97.72	29.39	13.08	33.58	21.88	159.05	22.19
Bhagwat et al. (2012) (12.5 mm ID)	41.94	60.67	61.83	35.15	211.71	171.97	83.92	1682.23	249.14
Xue et al. (2013) (65 mm ID)	73.09	72.77	86.32	78.7	46.72	61.41	67.66	202.92	42.69
Almabrok (2013) (101.6 mm ID)	89.17	89.27	77.75	90.95	69.24	73.83	83.71	145.21	65.17
Lu et al. (2018) (50.8 mm ID)	8.21	8.42	88.3	11.15	32.15	12.17	9.92	348.06	7.15
Ualiyeva et al. (2022) (50.8 mm ID) (μ_L= 4 cP)	96.6	70.28	76.79	37.65	131.55	59.25	48.12	1241.97	47.1
Ualiyeva et al. (2022) (50.8 mm ID) (μ_L= 7 cP)	266.6	51.54	65.46	48.49	242.4	43.09	103.49	1930.35	44.62
Bouyahiaoui et al. (2024) (34 mm ID)	69.08	63.54	87.84	73.55	44.32	89.4	60.1	281.97	53.62
Present study (30 mm ID)	23.15	22.96	82.35	28.74	56.69	23.58	25.27	628.54	19.92

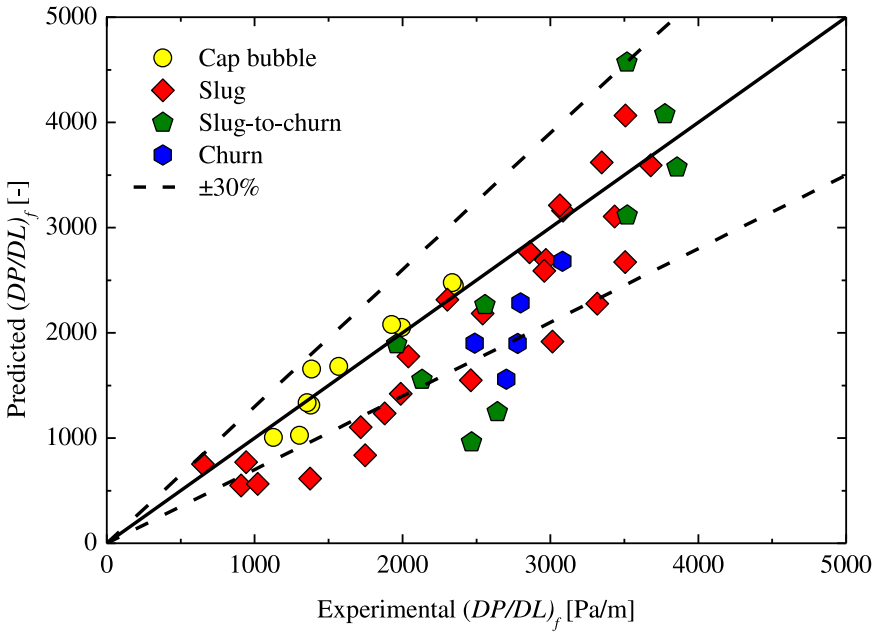

Fig. 23. Comparison between the experimental frictional pressure drop results and the prediction provided by the proposed model.

(2024) were not considered in this assessment study. One remark from the table that the predictions provided by each model were different for each dataset. It appears, therefore, that no general model performs well for all datasets. The proposed model provides the best predictions with the present database (*AARE*= 19.92 %) and data of Almabrok (2013) (*AARE*= 65.17 %) (which, remember, were used in its development). It also provides the lowest *AARE* with the datasets of Xue et al. (2013) and Lu et al. (2018). On the other hand, it gives the second-best prediction with the datasets of Bouyahiaoui et al. (2024) (after the model of Qiao et al. (2017) with $C = 100$), and Ualiyeva et al. (2022) for both μ_L= 4 cP (after the model of Qiao et al. (2017) with $C = 25$) and μ_L= 7 cP (just after the model of Yao et al. (2018)). These results show clearly the performance superiority of the proposed model to predict the collected datasets compared to other evaluated models. This statement is also interesting since, as was mentioned in Section 2, this is the first frictional pressure drop model for vertical downward flow that has been validated with independent data. However, its performance was low for the data obtained with a small diameter pipe of Lau and Razkallah (1995) (9.53 mm ID) and Bhagwat and Ghajar (2017) (12.5 mm ID). This can be explained by the difference in the lengths of the flow structures in small and moderate pipe diameters. Further experimental analysis will enable confirmation of this hypothesis.

Note also that the models proposed by Friedel (1979), Yao et al. (2018) and Qiao et al. (2017) also provide good predictions for a large number of datasets. With regard to the two values of C (25 and 100) proposed by Qiao et al. (2017), the authors explained that these values

depend on the inlet mixer device used. An inlet mixer equipped with a flow straightener or where the vertical downward flow is generated from a horizontal pipe (as in our setup) induces less disturbance and less turbulence, which induces a lower value of C. Interestingly, the correlation with $C = 25$ performs better than the correlation with $C = 100$ with the datasets from Lau and Rezkallah (1995) and Ualiyeva et al. (2022). With the data from Almabrok (2013) and Bouyahiaoui et al. (2024), on the other hand, the opposite is true. The experimental setups of all these studies comprise a vertical downward pipe after a vertical upward pipe through an inverted U-bend. Further research is therefore needed to more thoroughly analyze the influence of the inlet mixer on the performance of each model under different operating conditions. Note that the values of *AARE* in Table 7 are higher than those reported for liquid holdup assessment. This shows that modeling frictional pressure drop presents a greater challenge.

In Fig. 23 the cross-plot between the prediction from the proposed model and our results shows that the model slightly underestimates these results. This plot also shows that the best prediction is obtained with cap bubble flow. Moreover, most of these data are predicted within the ±30 % range, which can be considered highly satisfactory for two-phase flow pressure drop (Arabi et al., 2021; Cai et al., 2022; Höhn et al., 2025b). The difference in trends for the results for each flow regime in Fig. 23 clearly shows that the performance of the model depends on the nature of the flow regime. This observation, which was also highlighted in the recent study by Bouyahiaoui et al. (2024), is clearly seen in the table in Appendix C, where the performances of the models are evaluated by taking into account the nature of the flow regime.

5. Summary and conclusions

The aim of this study is to contribute to the prediction of liquid holdup and frictional pressure drop in vertical downward gas-liquid two-phase flow through an exploration of new modeling approaches. A new database was generated with an air-water mixture and a 30 mm ID pipe. The dataset generated covers the range of high-input liquid fraction, where cap bubble, slug, slug-to-churn and churn flows were observed. The main conclusions are summarized as follows:

1) For the three flow regimes studied, liquid holdup is influenced by both the liquid and gas superficial velocities.
2) Cap bubble-to-slug flow transition occur at $H_L = 0.82$-0.85, while slug-to-churn flow transitions occur in a wide range of liquid holdup values. This finding illustrates the difficulty in associating the latter transition with one critical value of liquid holdup.
3) The liquid holdup data show that both inertia- and buoyancy-driven flows are present in cap bubble and slug flows. The inertia-driven flow becomes more important with the transition to churn flow. On the other hand, increasing V_{SL} induces a shift in the transition to the inertia-driven flow.
4) Our results with the drift-flux model show that V_{SG}, V_{SL} and the nature of the flow regime influence the distribution coefficient.
5) Using the generated data and the database from the literature, we proposed a new approach based on $H_L V_{SG}/V_{SL}$ vs λ_L to model liquid holdup for downward flow. A sigmoid function was used to fit the data obtained for a wide range of experimental conditions. Despite its no-flow-regime-dependent nature, the advantage of the proposed correlation is that it considers the complex effect of flow regimes on the impact of V_{SL} and V_{SG} on liquid holdup.
6) The proposed liquid holdup model was evaluated with an experimental database made up of 1646 data points, including 1189 independent data, using the statistical parameter *AARE*. The model was found to give optimal performance for a wide range of experimental conditions and flow regimes. It also has the advantage to be applicable for a wide range of V_{SL} and V_{SG}.
7) Total pressure drop can be correlated with the mixture Froude number, where each flow regime must be considered independently.
8) Lockhart-Martinelli analysis showed the need to consider a fourth term for modeling frictional pressure drop using the separated approach in vertical downward flow. This analysis also showed the influence of the flow regimes on the frictional pressure drop behavior.
9) A new empirical model is proposed for predicting the pressure drop based on the fourth term due to the buoyancy effect. A new approach is used to correlate this term.
10) As indicated by the lowest values of *AARE*, the proposed frictional pressure drop model performs satisfactorily. Furthermore, it can accurately predict independent datasets from Sun et al. (2004a) and Lu et al. (2018), with *AARE* values of 22.19 % and 7.15 %, respectively, demonstrating its reliability.

CRediT authorship contribution statement

Abderraouf Arabi: Writing – original draft, Visualization, Validation, Software, Methodology, Investigation, Funding acquisition, Formal analysis, Data curation, Conceptualization. **Ronaldo Luis Höhn:** Writing – review & editing, Validation, Methodology. **Jordi Pallares:** Writing – review & editing, Visualization, Project administration, Funding acquisition. **Youssef Stiriba:** Writing – review & editing, Visualization, Project administration, Conceptualization.

Declaration of competing interest

The authors declare that they have no known competing financial interests or personal relationships that could have appeared to influence the work reported in this paper.

Acknowledgements

A. A. has received funding from the Beatriu de Pinós postdoctoral fellowship program (2021 BP 00052) funded by the Secretary of Universities and Research of the government of Catalonia and the European Union's Horizon 2020 Program for Research and Innovation under Marie Skłodowska-Curie grant agreement No. 801370. This work was supported through projects PID2020-113303GB-C21 and PID2023-146648NB-C21 funded by Spain's Ministerio de Ciencia e Innovación (MCIN) and Agencia Estatal de Investigación (AEI) and by project 2021SGR00732 of the Departament de Recerca i Universitats de la Generalitat de Catalunya. The authors appreciate the help of Daniel Graus Muñoz for the setup settings and would like to acknowledge Prof. Abdelwahid Azzi and Dr. Hiba Bouyahiaoui for their invaluable advice and shared data, respectively.

Supplementary materials

Supplementary material associated with this article can be found, in the online version, at doi:10.1016/j.ijmultiphaseflow.2025.105371.

Appendix A. Experimental database

The experimental data tables of liquid holdup and frictional pressure drop are attached as supplementary files.

Appendix B

Evaluation of the liquid holdup predictive models by considering the nature of the flow regime.

Datasource	Flow regime	Yamazaki and Yamaguchi (1979)	Clark and Flemmer (1984)	Hirao et al. (1986)	Kataoka and Ishii (1987)	Usui and Sato (1989)	Goda (2001)	Goda et al. (2003)	Wang et al. (2018)	Dong and Hibiki (2021)	Bouyahiaoui et al. (2020)	Shi et al. (2021) (Falling film flow)	Shi et al. (2021) (Annular Flow)	Shi et al. (2021) (Bubble flow)	Shi et al. (2021) (Slug flow)	Shi et al. (2021) (Transition flow)	Hwang et al. (2023)	Developed correlation
Tikhonenko (1973) (33 mm ID) ($P = 1.96$ MPa)	-	172.81	72.96	117.12	102.02	22.11	21.59	24.17	17.27	35.86	158.63	75.48	105.48	115.56	58.37	110.2	256.67	123.76
Tikhonenko (1973) (33 mm ID) ($P = 9.06$ MPa)	-	109.64	38.25	33.37	33.94	26.39	27.69	18.19	13.17	12.17	39.52	54.08	66.06	68.39	42.87	67.87	134.01	72.01
Usui and Sato (1989) (16 mm ID)	Bubble	2.50	2.11	9.43	1.20	7.31	9.43	9.77	19.53	8.39	11.91	3.64	2.22	2.20	5.25	2.22	2.46	5.24
	Slug	5.07	5.34	26.8	4.44	20.13	30.3	22.25	43.66	18.5	18.11	17.13	12.34	10.80	21.00	11.60	12.22	11.13
	Churn	41.65	9.89	51.5	33.62	55.67	51.5	55.1	81.81	20.75	14.34	13.78	26.37	30.11	12.60	28.13	47.87	26.96
	Annular	17.84	19.58	19.97	17.8	62.92	27.92	26.83	38.37	31.84	24.83	29.27	24.69	23.27	32.84	24.05	46.78	30.89
	Falling film	234.9	26.52	42.07	112.64	80.2	20.35	24.91	14.71	68.05	55.61	199.98	263.42	271.08	113.36	263.40	163.29	211.40
	All database	108.10	15.75	27.34	54.81	48.63	26.63	25.64	33.51	34.19	26.84	90.63	118.08	123.83	50.58	120.68	79.20	100.89
Usui and Sato (1989) (24 mm ID)	Bubble	1.92	2.08	1.83	2.89	3.56	1.83	2.74	2.74	1.72	11.10	2.28	3.12	3.40	1.73	3.25	3.71	3.64
	Slug	11.92	9.18	8.94	13.24	11.65	8.94	8.8	33.09	4.89	13.62	7.82	10.33	11.36	6.54	10.78	19.87	6.63
	Churn	88.75	51.43	39.06	74.63	13.86	39.06	42.62	65.03	27.99	12.85	68.93	86.44	91.26	51.32	88.71	89.22	72.68
	Annular	20.06	12.56	19.51	15.41	61.94	33.22	17.03	37.51	10.53	5.87	17.01	12.83	12.38	21.75	12.61	48.23	14.84
	Falling film	186.36	63.06	81.75	134.16	-	82.00	55.57	56.66	67.13	37.14	165.64	187.6	193.99	139.52	190.5	191.75	172.01
	All database	89.70	33.59	33.99	66.98	32.14	36.42	26.92	39.18	29.22	16.58	76.27	88.07	91.21	63.69	89.5	99.87	80.33
Roustan et al. (1992) (50 mm ID)	-	1.04	1.65	1.08	1.59	2.57	1.08	0.71	0.71	0.97	0.50	0.59	1.19	1.38	0.30	1.28	3.26	2.75
Jiang and Rezkallah (1993) (9.53 mm ID)	Bubble	6.42	8.58	8.11	9.11	8.48	7.45	8.60	7.15	6.94	10.49	7.35	7.70	7.81	7.10	7.75	10.11	7.88
	Bubble-slug	15.08	17.38	17.25	17.75	17.03	16.78	19.83	13.19	16.31	26.22	14.02	14.35	14.46	14.13	14.40	20.14	13.48
	Slug	31.31	21.14	31.94	32.38	20.03	28.55	28.02	17.85	17.01	21.44	17.08	22.11	23.81	16.91	22.86	46.01	21.39
	Churn	23.88	30.32	31.86	26.40	31.33	36.80	32.00	36.68	28.51	30.47	32.62	30.89	30.28	33.91	30.62	17.95	28.41
	Annular	190.44	471.38	559.52	567.38	403.18	215.64	230.93	199.23	96.83	716.51	239.5	252.31	258.31	230.65	254.02	1080.02	99.92
	Falling film	93.05	57.93	104.25	133.5	42.3	76.32	89.47	53.67	72.04	88.72	145.32	130.47	127.79	106.34	125.61	292.49	52.14
	All database	86.39	182.34	221.84	222.75	156.66	95.41	103.43	92.47	45.39	288.88	105.3	110.69	113.02	99.89	111.15	420.83	49.50
Kashinsky and Randin (1999) (42.3 mm ID)	Bubbly	0.95	1.34	4.48	1.41	11.38	4.48	6.06	4.17	4.27	6.07	0.60	1.33	1.64	0.98	1.49	1.64	2.13
Hernandez et al. (2002) (50.8 mm ID)	Annular	115.69	91.19	120.54	104.15	91.29	108.45	92.98	72.61	37.08	133.98	125.89	144	147.19	119.62	144.39	305.80	55.97
	Slug	28.70	17.74	23.82	22.03	54.91	15.02	16.03	12.73	13.75	29.73	19.81	22.25	23.04	18.10	22.59	65.77	12.11
	Bubble	17.75	16.8	19.79	19.02	26.02	17.01	16.47	13.50	6.59	23.54	19.61	20.76	21.12	18.78	20.91	40.11	8.44
	All database	57.47	44.35	53.42	50.51	38.06	44.26	40.93	30.24	18.38	62.66	56.32	65.51	68.77	51.79	67.53	146.71	27.25
Sun et al. (2004a) (50.8 mm ID)	Bubbly	1.39	0.61	1.46	0.72	2.68	1.37	1.59	1.59	1.42	4.96	0.49	0.41	0.41	0.71	0.42	0.48	0.35
	Bubbly-to-slug	2.13	0.71	1.26	0.73	2.67	1.32	1.15	1.15	1.619	1.21	0.61	0.56	0.62	0.68	0.59	1.94	2.29
	All database	1.62	0.64	1.40	0.72	2.67	1.35	1.46	1.46	1.48	3.80	0.53	0.45	0.48	0.70	0.47	0.93	0.95
Sun et al. (2004b) (50.8 mm ID)	Bubbly	2.13	1.18	2.93	1.47	5.59	2.68	3.33	3.33	2.76	11.94	0.85	0.6	0.68	1.32	0.64	0.64	0.48
	Bubbly-to-slug	2.23	0.47	1.65	0.48	3.25	1.30	1.43	1.43	1.96	1.49	0.36	0.26	0.36	0.55	0.31	1.93	3.66

(*continued on next page*)

(*continued*)

Datasource	Flow regime	Yamazaki and Yamaguchi (1979)	Clark and Flemmer (1984)	Hirao et al. (1986)	Kataoka and Ishii (1987)	Usui and Sato (1989)	Goda (2001)	Goda et al. (2003)	Wang et al. (2018)	Dong and Hibiki (2021)	Bouyahiaoui et al. (2020)	Shi et al. (2021) (Falling film flow)	Shi et al. (2021) (Annular Flow)	Shi et al. (2021) (Bubble flow)	Shi et al. (2021) (Slug flow)	Shi et al. (2021) (Transition flow)	Hwang et al. (2023)	Developed correlation
	All database	2.17	0.90	2.42	1.07	4.65	2.13	2.57	2.57	2.44	7.76	0.66	0.46	0.55	1.01	0.51	1.16	1.75
Ishii et al. (2004) (25.4 mm ID)	Bubbly	2.28	0.97	0.93	1.19	2.87	0.95	0.85	0.85	2.56	0.88	0.64	0.84	0.94	0.55	0.85	2.69	2.51
Ishii et al. (2004) (50.8 mm ID)	Bubbly	1.33	0.70	1.52	0.80	2.47	1.41	1.65	1.65	1.34	4.5	0.64	0.59	0.64	0.80	0.60	0.85	0.51
Bhagwat and Ghajar (2012, 2017) (12.7 mm ID)	Bubbly	8.41	8.01	19.74	4.63	12.2	20.95	17.15	26.1	17.54	13.89	14.24	11.75	10.97	16.23	11.37	1.63	16.22
	Slug	7.28	21.16	49.55	6.44	36.73	50.26	52.24	58.49	34.93	41.14	28.6	18.61	16.15	37.28	17.30	5.35	14.29
	Intermittent/ Froth	16.67	28.05	26.41	17.77	45.87	38.75	31.52	42.08	35.28	21.77	29.33	25.33	24.03	32.26	24.78	16.78	32.62
	Annular	23.01	17.42	17.69	18.52	46.21	19.12	19.72	28.97	70.19	31.14	14.13	13.11	13.06	15.29	13.04	94.91	51.41
	Falling film	29.64	30.36	22.72	18.61	64.72	36.07	34.56	45.65	57.58	29.63	36.45	44.42	45.51	34.45	44.93	60.28	44.18
	Transient	16.91	9.36	46.33	15.68	24.48	46.33	60.69	-	27.68	-	13.38	13.37	16.91	14.22	15.04	20.20	7.18
	All database	17.29	21.77	29.00	13.97	42.98	34.24	33.26	39.24	45.99	29.15	24.51	22.06	21.30	27.65	21.66	39.63	32.57
Vieira et al. (2015) (76 mm ID) (μ_L= 1 cP)	Annular	31.13	236.00	288.65	272.27	-	110.31	118.94	91.40	94.78	405.22	134.82	145.86	149.71	127.07	147.51	657.13	66.43
Vieira et al. (2015) (76 mm ID) (μ_L= 10 cP)	Annular	42.91	149.04	188.18	197.57	-	75.75	79.5	58.67	96.05	270.89	93.72	103.03	106.24	87.99	104.38	464.25	75.90
Almabrok et al. (2016)	Bubbly	3.94	5.62	4.24	3.96	5.91	4.24	3.79	5.29	3.72	3.36	5.20	5.54	5.64	4.85	5.58	8.90	6.80
	Intermittent	106.78	80.32	40.54	55.02	44.88	34.13	30.72	18.35	55.88	31.68	62.10	74.36	79.11	52.62	76.53	136.22	83.61
	Annular	202.66	229.04	294.5	244.99	-	170.35	169.57	139.84	41.85	354.97	201.33	225.33	234.53	187.19	229.6	643.9	110.53
	All database	157.78	165.75	179.51	162.54	35.60	107.98	107.16	90.47	43.68	220.15	140.32	159.65	166.71	126.9	162.91	437.39	94.35
Xue et al. (2016) (25 mm ID)	Bubbly	5.64	5.64	6.57	7.37	10.08	6.57	8.18	13.24	5.71	20.27	4.37	5.92	6.77	4.42	6.29	11.26	4.53
	Slug	7.96	6.59	16.39	9.52	18.73	16.59	13.34	24.39	8.31	10.76	6.10	4.70	4.75	8.57	4.71	19.14	3.38
	Churn	11.01	5.19	15.86	7.65	47.53	28.72	14.49	25	12.13	7.01	15.35	10.53	9.21	19.24	9.84	32.48	7.94
	Annular	60.88	66.86	96.96	93.71	89.15	79.40	72.34	61.93	30.08	114.26	90.03	92.06	93.21	87.6	92.48	243.59	24.44
	All database	27.38	26.7	40.68	37.58	42.72	40.63	33.39	36.46	17.31	45.47	38.37	36.82	37.34	38.51	36.69	101.82	12.71
Wang et al. (2018) (203.2 mm ID)	Annular	2076.68	1047.13	924.52	518.02	907.00	989.46	675.23	957.44	755.85	127.4	1641.18	2048.91	2166.44	1269.4	2103.96	1479.83	1882.71
	Cap bubbly	23.02	24.51	16.55	22.16	12.21	16.55	17.97	14.60	17.95	19.51	21.26	22.96	23.48	19.88	23.19	29.49	21.82
	Churn-turbulent	228.15	210.82	165.35	191.72	104.25	145.07	166.23	113.69	176.31	172.21	183.62	197.89	202.31	172.25	200.00	268.73	201.47
	All database	980.08	482.2	335.19	256.18	167.07	328.2	258.51	154.87	365.71	121.25	744.37	936.96	987.91	518.69	960.84	713.41	886.71
Li et al. (2018) (203.2 mm ID)	Cap bubbly	23.23	25.34	22.83	23.89	20.33	22.83	22.44	22.44	22.97	21.38	25.08	25.74	26.00	24.55	25.87	26.8	25.79
	Churn-turbulent	465.87	390.93	418.46	369.52	49.53	279.29	367.99	300.7	343.52	390.93	341.99	367.99	377.17	322.11	372.58	597.4	388.75
	Annular	3321.87	1390.29	1246.44	1191.82	2587.7	1734.07	1175.91	1685.6	1255.05	162.61	4034.36	4789.29	3717.03	1907.38	4855.75	1682.27	3144.91
	All database	2296.09	917.43	836.12	793.78	885.85	942.57	783.63	923.58	826.33	184.38	2494.03	2952.32	2545.21	1213.76	2993.14	1134.2	2165.70
Chalgeri and Jeong (2019) (D_h= 4.55 mm)	Bubbly	1.96	2.95	2.44	4.02	4.23	1.77	2.10	2.31	1.16	3.40	1.41	1.94	2.13	1.32	2.03	5.23	1.74
	Large bubbly	22.14	17.41	18.14	26.77	28.56	18.26	17.44	20.58	11.91	20.13	14.78	19.00	20.45	13.94	19.67	29.45	17.93
	Cap bubbly	12.86	15.64	16.24	19.63	20.15	11.28	14.47	11.00	3.25	15.81	13.81	15.32	15.84	12.95	15.54	27.67	2.43
	Slug	11.10	7.73	13.16	14.99	16.19	15.76	9.78	13.72	8.24	9.14	10.34	9.25	9.12	11.73	9.17	31.34	7.84
	Churn	11.67	6.72	15.58	10.46	11.81	23.32	14.01	22.87	13.70	10.28	17.00	15.06	14.44	18.75	14.74	35.06	9.88
	Annular	29.71	8.83	22.13	28.93	32.37	27.52	26.30	29.57	11.18	20.41	37.25	33.19	31.96	39.11	32.62	83.83	12.86
	Falling film	322.77	254.78	118.52	333.89	343.11	118.52	48.05	-	138.09	-	320.39	340.31	345.04	295.61	342.55	308.3	323.29
	Undefined	107.12	57.60	54.15	109.4	118.97	54.15	51.11	-	24.40	70.89	70.70	88.49	94.77	60.59	91.27	112.52	87.48
	All database	28.19	18.19	17.37	30.65	32.86	18.49	14.44	12.70	11.39	12.49	24.45	26.77	27.61	23.21	27.14	42.37	22.51
Hazuku et al. (2020) (1.03 mm ID)	Bubbly	1.52	21.65	5.05	1.44	1.86	5.15	13.34	13.34	5.10	0.31	1.37	1.72	1.82	0.93	1.75	1.17	1.36

(*continued on next page*)

(*continued*)

Datasource	Flow regime	Yamazaki and Yamaguchi (1979)	Clark and Flemmer (1984)	Hirao et al. (1986)	Kataoka and Ishii (1987)	Usui and Sato (1989)	Goda (2001)	Goda et al. (2003)	Wang et al. (2018)	Dong and Hibiki (2021)	Bouyahiaoui et al. (2020)	Shi et al. (2021) (Falling film flow)	Shi et al. (2021) (Annular Flow)	Shi et al. (2021) (Bubble flow)	Shi et al. (2021) (Slug flow)	Shi et al. (2021) (Transition flow)	Hwang et al. (2023)	Developed correlation
Hazuku et al. (2020) (3 mm ID)	Bubbly	1.24	1.08	3.33	0.36	0.42	3.33	8.59	1.47	3.31	5.21	0.47	0.44	0.44	0.77	0.46	0.50	0.41
Hazuku et al. (2020) (5 mm ID)	Bubbly	1.48	1.06	3.56	0.40	0.42	3.66	11.01	2.20	3.68	1.3	0.76	0.64	0.62	0.84	0.62	0.22	0.60
Bouyahiaoui et al. (2020) (34 mm ID)	Churn	46.2	25.33	24.84	32.49	60.10	39.85	14.58	40.69	14.82	10.00	23.58	21.08	21.45	26.64	21.27	72.74	29.72
Shi et al. (2021) (20 mm ID)	-	19.61	23.87	26.89	18.30	71.78	45.92	43.2	48.38	54.62	36.91	39.47	35.89	34.43	41.22	35.19	65.4	40.09
Olarinoye (2021)	Annular	61.96	236.53	291.36	257.14	-	200.1	197.89	152.39	82.65	382.84	238.31	255.54	261.39	225.95	258.13	670.05	20.62
Ualiyeva et al. (2022) (50.8 mm ID) (μ_L= 4 cP)	Annular	92.41	43.97	47.02	97.46	-	39.73	42.27	25.13	50.49	31.47	50.68	60.68	63.94	44.86	62.12	168.37	61.11
Ualiyeva et al. (2022) (50.8 mm ID) (μ_L= 7 cP)	Annular	108.83	58.74	55.39	115.62	-	56.79	55.39	52.39	63.52	47.23	65.5	74.53	78.63	57.79	76.34	191.63	74.99
Osuagwu (2024) (50.8 mm ID)	Slug	310.54	93.65	205.78	97.82	-	70.99	108.04	48.02	68.71	127.91	79.44	64.53	102.19	80.29	81.27	579.84	180.52
	Churn	78.40	81.81	105.21	99.75	-	90.22	83.00	51.34	58.29	116.55	115.46	125.43	128.76	107.12	126.96	329.29	25.76
	Annular	376.74	820.01	1001.22	931.03	-	740.34	751.53	519.08	95.94	1027.89	889.95	932.51	972.98	822.47	950.94	2257.55	144.56
	All database	197.76	244.14	354.20	281.52	-	254.30	260.81	174.20	63.58	345.8	291.36	294.44	307.61	282.83	299.91	800.79	88.25
Present study (30 mm ID)	Cap bubble	2.10	1.70	2.35	1.98	3.31	2.65	1.76	1.76	2.48	1.42	1.44	1.51	1.63	1.71	1.57	3.06	3.63
	Slug	6.24	5.72	4.91	6.67	11.1	8.40	5.23	9.92	7.67	4.99	6.18	5.94	5.99	6.58	5.98	11.93	8.65
	Slug to churn transition	21.34	18.62	6.03	22.08	14.6	7.99	7.43	12.24	10.18	11.53	8.50	12.29	13.52	6.14	12.88	36.32	15.80
	Churn	35.55	26.91	15.63	33.04	26.39	19.88	6.92	22.85	8.23	14.66	5.07	8.17	10.75	7.88	9.35	56.95	21.19
	All database	11.16	9.43	5.69	11.24	11.71	8.33	5.10	10.00	7.13	6.45	5.53	6.43	6.97	5.64	6.69	19.19	10.21

Appendix C

Evaluation of the frictional pressure drop predictive models by considering the nature of the flow regime.

Datasource	Flow regime	Yamazaki and Yamaguchi (1979)	Friedel (1979)	Lau and Rekallah (1995) Annular flow	Qiao et al. (2017) (C = 25)	Qiao et al. (2017) (C = 100)	Yao et al. (2018)	Lu et al. (2018)	Hwang et al. (2024)	Developed correlation
Roustan et al. (1992) (50 mm ID)	-	33.39	35.8	94.58	34.23	63.34	29.03	42.91	430.55	37.8
Lau and Rezkallah (1995) (9.53 mm ID)	Bubbly	23.75	31.36	96.22	29.97	109.39	17.57	55.40	705.42	28.15
	Bubbly-slug	15.41	30.57	82.17	6.74	123.73	16.65	45.74	984.73	6.92
	Slug	41.85	59.62	72.74	25.45	191.88	87.48	73.34	1564.15	99.5
	Froth	21.22	27.62	90.85	19.08	88.83	5.45	42.33	602.16	7.10
	Slug-annular	18.87	34.92	91.69	21.40	147.64	13.93	57.75	1177.70	52.44
	Annular	28.55	54.52	44.78	11.72	222.72	26.86	71.63	1890.82	162.1
	Falling film	31.33	59.18	38.74	30.51	189.83	42.35	66.53	1623.02	484.58
	All database	30.81	50.77	63.26	26.36	171.97	43.14	65.12	1394.85	231.78
Sun et al. (2004a) (50.8 mm ID)	Bubbly	31.52	29.67	98.75	29.73	16.22	33.57	23.33	130.79	20.77
	Bubbly-to-slug transition	27.15	24.61	95.4	28.63	6.01	33.61	18.61	222.62	25.38
	All database	30.18	28.12	97.72	29.39	13.08	33.58	21.88	159.05	22.19
Bhagwat et al. (2012) (12.5 mm ID)	Bubbly	61.10	81.86	86.97	65.74	219.81	54.22	117.1	1353.75	62.43
	Slug	30.49	39.42	85.68	24.63	152.93	27.78	56.84	1291.65	51.03
	Churn	60.65	81.17	33.05	21.69	281.9	109.33	105.07	2234.11	156.27
	Annular	27.42	75.12	21.45	16.68	306.47	609.32	107.95	2498.14	873.23
	Falling film	30.5	28.77	65.82	40.9	119.74	123.12	34.32	1286.34	196.04
	All database	41.94	60.67	61.83	35.15	211.71	171.97	83.92	1682.23	249.14
Xue et al. (2013) (65 mm ID)	Bubbly	61.95	59.3	98.01	61.42	39.51	65.8	54.11	121.75	33.74
	Slug	81.17	79.51	95.53	83.61	65.74	56.99	77.66	79.61	64.36
	Churn	70.09	71.02	78.51	78.77	36.22	63.37	63.91	293.99	30.86
	All database	73.09	72.77	86.32	78.7	46.72	61.41	67.66	202.92	42.69
Almabrok (2013) (101.6 mm ID)	Bubbly	91.37	90.93	98.49	92.07	86.81	92.39	90.32	48.12	63.72
	Intermittent	89.91	90.89	89.65	92.74	78.3	44.92	87.93	78.51	56.90
	Annular	88.67	88.46	71.01	90.11	63.95	84.06	81.39	181.27	68.70
	All database	89.17	89.27	77.75	90.95	69.24	73.83	83.71	145.21	65.17
Lu et al. (2018) (50.8 mm ID)	Bubbly	3.16	2.04	97.41	3.02	19.88	7.43	4.71	187.41	4.15
	Transitional	3.11	4.02	92.62	3.1	35.62	8.95	10.23	315.98	3.10
	Slug	25.99	25.82	68.36	39.42	35.74	24.93	14.37	588.92	20.29
	All database	8.21	8.42	88.3	11.15	32.15	12.17	9.92	348.06	7.15
Ualiyeva et al. (2022) (50.8 mm ID) (μ_L= 4 cP)	Annular	96.60	70.28	76.79	37.65	131.55	59.25	48.12	1241.97	47.10
Ualiyeva et al. (2022) (50.8 mm ID) (μ_L= 7 cP)	Annular	266.6	51.54	65.46	48.49	242.4	43.09	103.49	1930.35	44.62
Bouyahiaoui et al. (2024) (34 mm ID)	Bubbly	29.84	27.10	99.26	25.42	16.82	30.7	17.39	195.37	22.05
	Cap bubble	47.96	43.52	97.69	45.00	23.6	52.04	33.26	249.51	38.2
	Slug	67.85	63.83	93.98	70.93	43.71	58.71	61.52	214.79	67.21
	Churn	53.94	51.32	75.35	66.62	33.67	52.38	42.76	531.72	40.81
	Falling film	85.11	74.93	92.25	87.57	57.02	106.9	76.42	214.3	57.41
	Annular	73.30	68.58	83.69	77.82	47.07	137.19	65.11	246.27	54.24
	All database	69.08	63.54	87.84	73.55	44.32	89.4	60.1	281.97	53.62
Present study (30 mm ID)	Cap bubble	12.13	15.3	93.16	11.69	68.71	10.58	25.95	542.48	8.59
	Slug	21.16	20.98	82.08	25.93	54.83	27.6	22.81	636.48	21.94
	Slug to churn	29.67	27.32	73.28	39.19	67.07	21.49	27.24	729.87	23.65
	Churn	43.39	40.36	78.41	58.05	23.2	33.19	32.66	578.59	25.8
	All database	23.15	22.96	82.35	28.74	56.69	23.58	25.27	628.54	19.92

Data availability

The data will be shared as an Supplementary Material

References

Abdulkadir, M., Kajero, O.T., Olarinoye, F.O., Udebhulu, D.O., Zhao, D., Aliyu, A.M., Al-Sarkhi, A., 2021. Investigating the behaviour of air–water upward and downward flows: are you seeing what I Am seeing? Energies 14 (21), 7071.

Achour, B., Bedjaoui, A., Khattaoui, M., Debabeche, M., 2002. Contribution au calcul des écoulements uniformes à surface libre et en charge (Première partie). LARHYSS J. P-ISSN 1112-3680/E-ISSN 2521-9782 (1).

Almabrok, A.A., 2013. Gas-Liquid two-phase flow in up and down vertical pipes. PhD thesis, Cranfield university, Cranfield, U.K.

Almabrok, A.A., Aliyu, A.M., Lao, L., Yeung, H., 2016. Gas/liquid flow behaviours in a downward section of large diameter vertical serpentine pipes. Int. J. Multiph. Flow 78, 25–43.

Alsarkhi, A., Sarica, C., Pereyra, E., 2024. Novel correlations for the liquid holdup in a gas-liquid slug flow. Geoenergy Sci. Eng. 237, 212825.

Arabi, A., Salhi, Y., Zenati, Y., Si-Ahmed, E.K., Legrand, J., 2021. A discussion on the relation between the intermittent flow sub-regimes and the frictional pressure drop. Int. J. Heat Mass Transf. 181, 121895.

Altshul, A.D., 1952. "Obobshchonnaya Zavisi - most dlyagidravlicheskovo raschota turboprovodor" (Generalized formula for hydraulic analysis of pipes). Gidrotekhnicheskeye stroyitelstve 6, 44–47.

Ayegba, P.O., Sebilleau, J., Colin, C., 2022. Hydrodynamics of vertical upward and downward flow boiling in a millimetric tube. Int. J. Multiph. Flow 153, 104120.

Ayegba, P.O., Sebilleau, J., Colin, C., 2024a. Experimental investigation and modelling of hydrodynamics and heat transfer in flow boiling in normal and microgravity conditions. Int. J. Multiph. Flow 181, 104991.

Ayegba, P.O., Sebilleau, J., Colin, C., 2024b. Theoretical modeling of heat transfer in vertical upward and downward annular flow boiling. Heat Transf. Eng. 45 (4–5), 381–398.
Ayegba, P.O., Sebilleau, J., Colin, C., 2025. Modelling of wave velocity, wave frequency and interfacial friction factor in vertical upward and downward annular flow. Int. J. Heat Mass Transf. 247, 127157.
Barnea, D., 1987. A unified model for predicting flow-pattern transitions for the whole range of pipe inclinations. Int. J. Multiph. Flow 13 (1), 1–12.
Bhagwat, S.M., Ghajar, A.J., 2012. Similarities and differences in the flow patterns and void fraction in vertical upward and downward two phase flow. Exp. Therm. Fluid Sci. 39, 213–227.
Bhagwat, S.M., Ghajar, A.J., 2017. Experimental investigation of non-boiling gas-liquid two phase flow in downward inclined pipes. Exp. Therm. Fluid Sci. 89, 219–237.
Bhagwat, S.M., Mollamahmutoglu, M., Ghajar, A.J., 2012. Experimental investigation and performance evaluation of isothermal frictional two phase pressure drop correlations in vertical downward gas-liquid two phase flow. In: Heat Transfer Summer Conference, 44786. American Society of Mechanical Engineers, pp. 337–348.
Blasius, H., 1913. Das aehnlichkeitsgesetz bei reibungsvorgängen in flüssigkeiten. Mitteilungen über Forschungsarbeiten auf dem Gebiete des Ingenieurwesens: insbesondere aus den Laboratorien der technischen Hochschulen. Springer Berlin Heidelberg, Berlin, Heidelberg, pp. 1–41.
Blinkov, V.N., Melikhov, O.I., Melikhov, V.I., Kapustin, A.V., Dolganov, K.S., Tomashchik, D.Y., Selkin, S.S., 2022. Investigation on the interphase drag and wall friction in vertically oriented upward and downward two-phase flows under accident conditions in light water reactors. Nucl. Eng. Des. 389, 111666.
Bouyahiaoui, H., Azzi, A., Zeghloul, A., Hasan, A.H., Al-Sarkhi, A., Parsi, M., 2020. Vertical upward and downward churn flow: similarities and differences. J. Nat. Gas Sci. Eng. 73, 103080.
Bouyahiaoui, H., Azzi, A., Zeghloul, A., Hasan, A., Berrouk, A.S., 2018. Experimental investigation of a vertically downward two-phase air-water slug flow. J. Pet. Sci. Eng. 162, 12–21.
Bouyahiaoui, H., Saidj, F., Arabi, A., Al-Sarkhi, A., Azzi, A., 2024. Vertically downward gas-liquid flow: void fraction and pressure drop. Int. J. Multiph. Flow 172, 104711.
Cai, Q., D'Auria, F., Umminger, K., Bestion, D., Shan, J., 2022. Prioritizing pressure drop research in nuclear thermal hydraulics. Prog. Nucl. Energy 153, 104358.
Chalgeri, V.S., Jeong, J.H., 2019. Flow regime identification and classification based on void fraction and differential pressure of vertical two-phase flow in rectangular channel. Int. J. Heat Mass Transf. 132, 802–816.
Chisholm, D., 1967. A theoretical basis for the Lockhart-Martinelli correlation for two-phase flow. Int. J. Heat Mass Transf. 10 (12), 1767–1778.
Cioncolini, A., Thome, J.R., 2010. Predict. Entrain. Liq. Fraction Vert.
Cioncolini, A., Thome, J.R., 2012. Entrained liquid fraction prediction in adiabatic and evaporating annular two-phase flow. Nucl. Eng. Des. 243, 200–213.
De Winter, J.C., 2013. Using the student's" t"-test with extremely small sample sizes. Pract. Assess. Res. Eval. 18 (10), n10.
Clark, N.N., Flemmer, R.L.C., 1984. On vertical downward two phase flow. Chem. Eng. Sci. 39 (1), 170–173.
Devore, J.L., Carlton, M.A., 2016. Probability and Statistics for Engineering and the Sciences: Student Solutions Manual. Cengage Learning.
Dong, C., Hibiki, T., 2021. Drift-flux parameter modeling of vertical downward gas–liquid two-phase flows for interfacial drag force formulation. Nucl. Eng. Des. 378, 111185.
Dong, C., Rassame, S., Zhang, L., Hibiki, T., 2020. Drift-flux correlation for upward two-phase flow in inclined pipes. Chem. Eng. Sci. 213, 115395.
Drew, T.B., Koo, E.C., McAdams, W.H., 1932. The friction factor for clean round pipes. Trans. AIChE 28, 56–72.
Fang, X., Xu, Y., Zhou, Z., 2011. New correlations of single-phase friction factor for turbulent pipe flow and evaluation of existing single-phase friction factor correlations. Nucl. Eng. Des. 241 (3), 897–902.
Friedel, L., 1979. Improved friction pressure drop correlations for horizontal and vertical two-phase pipe flow. In: European Two-Phase Flow Group Meeting. Ispra, Italy.
Genić, S., Arandjelović, I., Kolendić, P., Jarić, M., Budimir, N., 2011. A review of explicit approximations of Colebrook's equation. FME Trans. 39, 67–71.
Goda, H., 2001. 'Flow regimes and local parameter measurements for downward two-phase flow,'' MS thesis. School of Nuclear Engineering. Purdue University, West Lafayette, IN, USA.
Goda, H., Hibiki, T., Kim, S., Ishii, M., Uhle, J., 2003. Drift-flux model for downward two-phase flow. Int. J. Heat Mass Transf. 46 (25), 4835–4844.
Hammer, M., Deng, H., Liu, L., Langsholt, M., Munkejord, S.T., 2021. Upward and downward two-phase flow of CO2 in a pipe: comparison between experimental data and model predictions. Int. J. Multiph. Flow 138, 103590.
Hazuku, T., Ihara, T., Hibiki, T., 2020. Measurement of local two-phase flow parameters of downward bubbly flow in mini pipes. Exp. Comput. Multiph. Flow 2, 89–98.
Hernandez, A., Gonzalez, L., Gonzalez, P., 2002. Experimental research on downward two-phase flow. SPE Annual Technical Conference and Exhibition? SPE. SPE-77504.
Hibiki, T., Ishii, M., 2003. One-dimensional drift–flux model for two-phase flow in a large diameter pipe. Int. J. Heat Mass Transf. 46 (10), 1773–1790.
Hirao, Y., Kawanishi, K., Tsuge, A., Kohriyama, T., 1986. Experimental study on drift flux correlation formulas for two-phase flow in large diameter tubes. In: Proceedings of 2nd International Topical Meeting on Nuclear Power Plant Thermal Hydraulics and Operations. Tokyo, Japan, 1-88-1-94.
Höhn, R.L., Arabi, A., Ballesta, S.V.V., Sassi, P.J., Pallarès, J., Stiriba, Y., 2025a. Analysis of flow regimes and volumetric phase fraction of vertical upward gas–liquid–solid three-phase flow. Can. J. Chem. Eng., (Artic. press).
Höhn, R.L., Arabi, A., Ballesta, S.V.V., Sassi, P.J., Pallarès, J., Stiriba, Y., 2025b. Effect of solid particles on the hydrodynamics of vertical upward gas–liquid two-phase flow: pressure drop analysis. Chem. Eng. Res. Des. 214, 234–250.
Hwang, D., Choi, N., Jung, W., Kim, T., Lee, Y., Jo, H., 2023. Plant-scale experiments of an air inflow accident under sub-atmospheric pressure by pipe break in an open-pool type research reactor. Nucl. Eng. Technol. 55 (5), 1604–1615.
Hwang, D., Kang, S.H., Choi, N., Jo, H., 2024. Development of a one-dimensional system code for the analysis of downward air-water two-phase flow in large vertical pipes. Nucl. Eng. Technol. 56 (1), 19–33.
Ishii, M., Paranjape, S.S., Kim, S., Sun, X., 2004. Interfacial structures and interfacial area transport in downward two-phase bubbly flow. Int. J. Multiph. Flow 30 (7–8), 779–801.
Jiang, Y., Rezkallah, K.S., 1993. A study on void fraction in vertical co-current upward and downward two-phase gas-liquid flow—I: experimental results. Chem. Eng. Commun. 126 (1), 221–243.
Jukić, D., Scitovski, R., 1996. The existence of optimal parameters of the generalized logistic function. Appl. Math. Comput. 77 (2–3), 281–294. https://doi.org/10.1016/s0096-3003(95)00251-0.
Kashinsky, O.N., Randin, V.V., 1999. Downward bubbly gas–liquid flow in a vertical pipe. Int. J. Multiph. Flow 25 (1), 109–138.
Kataoka, I., Ishii, M., 1987. Drift flux model for large diameter pipe and new correlation for pool void fraction. Int. J. Heat Mass Transf. 30 (9), 1927–1939.
Kyurkchiev, N., Markov, S., 2015. Sigmoid functions: some approximation and modelling aspects. LAP LAMBERT Academic Publishing, Saarbrucken, p. 4.
Lau, V., Rezkallah, K.S., 1995. New data on two-phase water-air hydrodynamics in vertical upward and downward tubes. In: 35th annual conference of the Canadian Nuclear Association and 16th annual conference of the Canadian Nuclear Society. Saskatoon (Canada), pp. 4–7. Jun 1995.
Lelouvetel, J., Tanaka, T., Sato, Y., Hishida, K., 2014. Transport mechanisms of the turbulent energy cascade in upward/downward bubbly flows. J. Fluid Mech. 741, 514–542.
Li, N., Chen, B., 2024. Investigation on gas-liquid two-phase frictional pressure drop in pipeline riser. Geoenergy Sci. Eng. 234, 212627.
Li, R., Nadarajah, S., 2020. A review of Student'st distribution and its generalizations. Empir. Econ. 58, 1461–1490.
Li, Z., Wang, G., Yousaf, M., Yang, X., Ishii, M., 2018. Flow structure and flow regime transitions of downward two-phase flow in large diameter pipes. Int. J. Heat Mass Transf. 118, 812–822.
Lokanathan, M., Hibiki, T., 2018. Flow regime transition criteria for co-current downward two-phase flow. Prog. Nucl. Energy 103, 165–175.
Lu, C., Kong, R., Qiao, S., Larimer, J., Kim, S., Bajorek, S., Hoxie, C., 2018. Frictional pressure drop analysis for horizontal and vertical air-water two-phase flows in different pipe sizes. Nucl. Eng. Des. 332, 147–161.
Márquez-Torres, L., Ochoa-Pineda, J., Pico, P., Valdés, J.P., Becerra, D., Pinilla, A., Ratkovich, N., 2020. Comparison of 63 different void fraction correlations for different flow patterns, pipe inclinations, and liquid viscosities. SN Appl. Sci. 2, 1–24.
Martin, C.S., 1976. Vertically downward two-phase slug flow. J. Fluids Eng. 98 (4), 715–722.
Mena, D.N., 2016. Inlet-induced Effects on Vertical Co-current Downward Air-water Twophase Flow. Master Thesis. The Pennsylvania State University, USA.
Moffat, R.J., 1988. Describing the uncertainties in experimental results. Exp. Therm. Fluid Sci. 1 (1), 3–17.
Montgomery, D.C., Runger, G.C., 2010. Applied Statistics and Probability for Engineers. John Wiley & Sons.
Moody, L.F., 1947. An approximate formula for pipe friction factors. Trans. ASME 69 (12), 1005–1011.
Muzychka, Y.S., .& Awad, M.M. (.2010). Asymptotic generalizations of the Lockhart–Martinelli method for two phase flows.
Olarinoye, F.O., 2021. Investigating the Behaviour of Two-Phase Vertical Upward and Downward flows in Large Diameter Pipe. Master thesis. African University of Science and Technology, Abuja F.C.T, Nigeria.
Osuagwu, O.C., 2024. Theoretical and Experimental Analysis of Downward Liquid-Gas Flow in Vertical Tubulars. Master's thesis. University of Oklahoma–Graduate College, USA.
Pereyra, E., Torres, C., 2005. FLOPATN—Flow pattern prediction and plotting computer code. The University of Tulsa, Tulsa, OK.
Qiao, S., Kim, S., 2018. On the prediction of two-phase pressure drop across 90° vertical elbows. Int. J. Multiph. Flow 109, 242–258.
Qiao, S., Li, J., Ren, J., Kim, S., 2022. Experimental investigation on effects of flow orientation on interfacial structure of air–water two-phase flow. Coatings 13 (1), 5.
Qiao, S., Mena, D., Kim, S., 2017. Inlet effects on vertical-downward air–water two-phase flow. Nucl. Eng. Des. 312, 375–388.
Rassame, S., Hibiki, T., 2018. Drift-flux correlation for gas-liquid two-phase flow in a horizontal pipe. Int. J. Heat Fluid Flow 69, 33–42.
Ren, J., Wang, H., 2023. Mathematical Methods in Data Science. Elsevier.
Roustan, M., Line, A., Wable, O., 1992. Modeling of vertical downward gas-liquid flow for the design of a new contactor. Chem. Eng. Sci. 47 (13–14), 3681–3688.
Ryan, D., Kang, D., Quan, Z., Dix, A., Kim, S., 2024. Experimental study and model assessment for void fraction in different orientations and flow regimes in air-water two-phase flows. Geoenergy Sci. Eng., 213531
Saidj, F., Arabi, A., Bouyahiaoui, H., Azzi, A., Hasan, A.H., 2025. Slug void fraction in vertical downward gas–liquid two-phase flow. Phys. Fluids 37 (1).
Sassi, P., Pallarès, J., Stiriba, Y., 2020a. Visualization and measurement of two-phase flows in horizontal pipelines. Exp. Comput. Multiph. Flow 2, 41–51.

Sassi, P., Stiriba, Y., Lobera, J., Palero, V., Pallares, J., 2020b. Experimental analysis of gas–liquid–solid three-phase flows in horizontal pipelines. Flow Turbul. Combust. 105, 1035–1054.
Sassi, P., Fernandez, G., Stiriba, Y., Pallares, J., 2022. Effect of solid particles on the slug frequency, bubble velocity and bubble length of intermittent gas–liquid two-phase flows in horizontal pipelines. Int. J. Multiph. Flow 149, 103985.
Schmid, D., Verlaat, B., Petagna, P., Schiffmann, J., Revellin, R., 2022. Adiabatic two-phase pressure drop of carbon dioxide in different channel orientations. Int. J. Heat Fluid Flow 95, 108966.
Shi, S., Wang, Y., Qi, Z., Yan, W., Zhou, F., 2021. Experimental investigation and new void-fraction calculation method for gas–liquid two-phase flows in vertical downward pipe. Exp. Therm. Fluid Sci. 121, 110252.
Sun, X., Paranjape, S., Ishii, M., Uhle, J., 2004a. LDA measurement in air–water downward flow. Exp. therm. fluid sci. 28 (4), 317–328.
Sun, X., Paranjape, S., Kim, S., Ozar, B., Ishii, M., 2004b. Liquid velocity in upward and downward air–water flows. Ann. Nucl. Energy 31 (4), 357–373.
Tikhonenko, L.K. (1973). "Influence of wall roughness and flow direction on the characteristics of two-phase adiabatic flow", in "achievements in research on heat transfer and hydraulics of two-phase flow in the elements of power generating equipment", pp. 109-119, Science, Moscow, 1973. (In Russian).
Ualiyeva, G., Pereyra, E., Sarica, C., 2022. An experimental study on two-phase downward flow of medium viscosity oil and air. SPE Annual Technical Conference and Exhibition? SPE. D021S021R006.
Usui, K., Sato, K., 1989. Vertically downward two-phase flow,(I) void distribution and average void fraction. J. Nucl. Sci. Technol. 26 (7), 670–680.
Vieira, R.E., Parsi, M., McLaury, B.S., Shirazi, S.A., Torres, C.F., Schleicher, E., Hampel, U., 2015. Experimental characterization of vertical downward two-phase annular flows using wire-mesh sensor. Chem. Eng. Sci. 134, 324–339.
Vijayan, P.K., Patil, A.P., Pilkhwal, D.S., Saha, D., Venkat Raj, V., 2000. An assessment of pressure drop and void fraction correlations with data from two-phase natural circulation loops. Heat Mass Transf. 36 (6), 541–548.
Wang, G., Li, Z., Yousaf, M., Yang, X., Ishii, M., 2018. Experimental study on vertical downward air-water two-phase flow in a large diameter pipe. Int. J. Heat Mass Transf. 118, 919–930.
Woldesemayat, M.A., Ghajar, A.J., 2007. Comparison of void fraction correlations for different flow patterns in horizontal and upward inclined pipes. Int. J. Multiph. Flow 33 (4), 347–370.
Xue, Y., Li, H., Hao, C., Yao, C., 2016. Investigation on the void fraction of gas–liquid two-phase flows in vertically-downward pipes. Int. Commun. Heat Mass Transf. 77, 1–8.
Xue, Y., Li, H., Sheng, T., Liao, C., 2013. Experimental investigation on flow patterns and frictional pressure drop of downward air-water two-phase flow in vertical pipes. Heat Transfer Summer Conference (Vol. 55485. American Society of Mechanical Engineers. V002T07A003.
Yamazaki, Y., Yamaguchi, K., 1979. Characteristics of cocurrent two-phase downflow in tubes: flow pattern, void fraction and pressure drop. J. Nucl. Sci. Technol. 16 (4), 245–255.
Yao, C., Li, H., Xue, Y., Liu, X., Hao, C., 2018. Investigation on the frictional pressure drop of gas liquid two-phase flows in vertical downward tubes. Int. Commun. Heat Mass Transf. 91, 138–149.
Zuber, N., Findlay, J., 1965. Average volumetric concentration in two-phase flow systems. J. Heat Transf. 87 (4), 453–468.